Precipitation in aqueous mixtures with addition of a strongly hydrophilic or hydrophobic solute

Ryuichi Okamoto and Akira Onuki
Department of Physics, Kyoto University, Kyoto 606-8502, Japan
(Received 8 October 2010; published 18 November 2010)

We examine phase separation in aqueous mixtures due to preferential solvation with a low-density solute (hydrophilic ions or hydrophobic particles). For hydrophilic ions, preferential solvation can stabilize water domains enriched with ions. This precipitation occurs above a critical solute density n_p in wide ranges of the temperature and the average composition, where the mixture solvent would be in a one-phase state without solute. The volume fraction of precipitated domains tends to zero as the average solute density $\bar{n}$ is decreased to n_p or as the interaction parameter χ is decreased to a critical value χ_p. If we start with one-phase states with $\bar{n}>n_p$ or $\chi>\chi_p$, precipitation proceeds via homogeneous nucleation or via heterogeneous nucleation, for example, around suspended colloids. In the latter case, colloid particles are wrapped by thick wetting layers. We also predict a first-order prewetting transition for $\bar{n}$ or χ slightly below n_p or χ_p for neutral colloids.

DOI: 10.1103/PhysRevE.82.051501 PACS number(s): 82.45.Gj, 61.20.Qg, 64.75.Cd, 81.16.Dn

I. INTRODUCTION

In fluid mixtures composed of water and a less polar organic liquid, phase separation behavior can be drastically changed by a small amount of salt [1–8]. With addition of a 10^{-3} mole fraction of hydrophilic salt like NaCl, the coexistence curve is typically shifted by a few kelvins upward in the upper critical solution temperature (UCST) case or downward in the lower critical solution temperature (LCST) case. In some aqueous mixtures, even if they are miscible at all T at atmosphere pressure without salt, addition of a small amount of salt gives rise to re-entrant phase separation behavior [3–6].

With ions added, moreover, many groups have also found long-lived heterogeneities (sometimes extending over a few micrometers) in one-phase states [9] and a third phase visible as a thin solidlike plate at a liquid-liquid interface in two-phase states [10]. A representative system is a mixture of H_2O (or D_2O), trimethylpyridine (3MP), and NaBr. The heterogeneities have been detected by dynamic light scattering [11], indicating spontaneous formation of aggregates or domains with small diffusion constants. Their typical radius is of order 10^3 Å at very small volume fractions. The third phase has been observed also in isobutylic acid (IBA)-water mixtures without added salt, where the isobutyric acid partly dissociates into butyrate$^-$ and H^+ ions. In addition, a drastic decrease in the ion mobility was observed in IBA-water for high contents of IBA [12]. Recently, mesophases have been observed when sodium tetraphenylborate $NaBPh_4$ was added to D_2O-3MP at about 0.1 M [13]. This salt dissociates into hydrophilic Na^+ and hydrophobic BPh_4^-. The latter ion consists of four phenyl rings bonded to an ionized boron.

Dramatic ion effects are ubiquitous in various soft materials such as polymers, gels, colloids, and mixtures containing ionic surfactants. For example, complex effects are known to be induced in polyelectrolytes when a second fluid component (cosolvent) is added to water. In particular, precipitation of DNA has been widely observed with addition of alcohol such as ethanol to water [14]. Here, the alcohol added is excluded from condensed DNA, which suggests solvation-induced wetting of DNA by water. We also mention observations of crystal formation of micron-sized water-rich droplets in a less polar oil-rich phase with addition of HBr [15]. The mechanism of this ordering was ascribed to the Coulomb interaction due to asymmetric partitioning of cations and anions in water and oil [16].

In these phenomena, the solvation (or hydration) interaction among ions and polar molecules should play a major role. Small hydrophilic ions are solvated by several water molecules [17–19], and the resultant solvation chemical potential per ion much exceeds the thermal energy k_BT and strongly depends on the ambient composition of the solvent. On the contrary, some hydrophobic particles dislike to be in contact with water molecules, which tend to form aggregates in water and are more soluble in oil than in water. In aqueous mixtures, a hydrophobic ion should be surrounded by oil molecules, which explains the mesophase formation observed by Sadakane *et al.* [13]. Hydrophilic and hydrophobic particles strongly affect the surrounding hydrogen bonding network in different manners [17] and the solvation is highly cooperative. Furthermore, when a small amount of water was added to methanol-cyclohexane, the coexistence curve was largely shifted [20] and a water-induced methanol-rich wetting layer appeared (which was nonexistent without water) [21]. These findings indicate strongly selective molecular interactions between water and the two components.

Obviously, the preferential solvation should strongly affect the phase transition behavior in aqueous mixtures with a small amount of a hydrophilic or hydrophobic solute, although this aspect has not been well studied. Recently, some efforts have been made to elucidate the solvation effects in phase separation in mixture solvents in electrolytes [22–28], polyelectrolytes [29], and ionic surfactants [30]. A review on the static properties was presented [31]. In the dynamics, a number of problems still remain unexplored [27,28].

In this paper, we present a theory of solvation-induced phase separation with a hydrophilic or hydrophobic solute. Thus, we aim to explain the observed heterogeneities in aqueous mixtures [9]. We may suppose hydrophilic monovalent ion pairs such as Na^+ and Cl^- in a binary mixture of water and a less polar component (called oil). As is well known, hydrophilic ions induce clustering of water molecules around them on microscopic scales, forming a solva-

tion shell [17–19]. We shall see that strongly hydrophilic ions can moreover induce formation of water-rich domains on macroscopic scales for sufficiently strong preference of water over oil. This can occur even when the mixture is outside the coexistence curve without ions.

The organization of this paper is as follows. In Sec. II, two-phase coexistence induced by the preferential solvation will be studied numerically and theoretically, where the electrostatic interaction does not appear explicitly. In Sec. III, inhomogeneous profiles such as interfaces will be calculated. We will show that a precipitated droplet can be stable only above a minimum radius due to the surface tension effect and that a solvation-induced prewetting transition occurs far from the coexistence curve without solute. In Sec. IV, two-phase coexistence with hydrophilic ions will be examined in the presence of the charge effect. In Sec. V, we will investigate the precipitation from one-phase states taking place as homogeneous nucleation. In Sec. VI, we will investigate adsorption and precipitation on colloid surfaces.

II. PHASE SEPARATION WITH STRONGLY SELECTIVE SOLUTE

Neglecting electrostatic interaction but accounting for the solvation interaction, we first consider a binary mixture composed of water and a less polar component in a cell with a fixed volume V. The second component will be simply called oil hereafter. Ions will be treated as a dilute third component (solute) with density $n(\boldsymbol{r})$. We may also suppose strongly hydrophilic or hydrophobic neutral particles (possibly with a complex structure) added in an aqueous binary mixture. Such particles can be solvated by a certain number of water or oil molecules depending on whether they are hydrophilic or hydrophobic.

In the following, we will suppose hydrophilic ions or particles. However, our results can be equally applicable to hydrophobic ions or particles if water and oil are exchanged (or ϕ is replaced with $1-\phi$). The Boltzmann constant k_B will be set equal to unity.

A. Conditions of two-phase coexistence with solute

The volume fractions of water, oil, and solute are written as $\phi(\boldsymbol{r})$ and $\phi'(\boldsymbol{r})$, and $v_I n(\boldsymbol{r})$, respectively, where v_I is the solute volume. If the two solvent species have the same molecular volume v_0, their densities are ϕ/v_0 and ϕ'/v_0. The solvent diameter is of order $a=v_0^{1/3}$. The space-filling condition is written as

$$\phi + \phi' + v_I n = 1. \tag{2.1}$$

The solute volume fraction is assumed to be small or $v_I n \ll 1$. This is more easily satisfied if the solute size is smaller than that of solvent or $v_I < v_0$. In this paper, to simplify the calculations, we thus set

$$\phi' = 1 - \phi. \tag{2.2}$$

The free-energy density $f_{\rm tot}(\phi,n)$ for the composition ϕ and the solute density n consists of three parts as

$$f_{\rm tot}(\phi,n) = f(\phi) + Tn\,\ln(n\lambda^3) - Tgn\phi. \tag{2.3}$$

The first term is assumed to be of the Bragg-Williams form for a fluid mixture [32],

$$f(\phi) = \frac{T}{v_0}[\phi\,\ln\,\phi + (1-\phi)\ln(1-\phi) + \chi\phi(1-\phi)], \tag{2.4}$$

where χ is the interaction parameter dependent on T. The length $a=v_0^{1/3}$ represents the molecular diameter (~ 3 Å for water). In Eq. (2.3), the second term arises from the solute translational entropy. λ is the thermal de Broglie length (but the terms linear in n are irrelevant and λ^3 may be replaced with v_0 in the following). The third term arises from the solute preference of water over oil. The parameter g is assumed to much exceed unity ($\gg 1$) [23]. We fix the average densities of the constituent components, which are expressed as

$$\bar{\phi} = \int d\boldsymbol{r}\phi/V, \quad \bar{n} = \int d\boldsymbol{r}n/V. \tag{2.5}$$

In our theory, χ, $\bar{\phi}$, and $\bar{n}$ are relevant control parameters. Changing χ through the critical value $\chi_c=2$ is equivalent to changing T through the solvent critical temperature T_c.

In two-phase coexistence in equilibrium, let the composition and the solute density be (ϕ_α,n_α) and (ϕ_β,n_β) in phases α and β with $\phi_\beta<\bar{\phi}<\phi_\alpha$ and $n_\beta<\bar{n}<n_\alpha$. Here, we give simple thermodynamic arguments. We define the chemical potentials as $h=\partial f_{\rm tot}/\partial\phi$ and $\mu=\partial f_{\rm tot}/\partial n$. From Eq. (2.3) we obtain

$$h = f'(\phi) - Tgn, \tag{2.6}$$

$$\mu = T[\ln(n\lambda^3) + 1 - g\phi], \tag{2.7}$$

where $f'=\partial f/\partial\phi$. First, the homogeneity relation $\mu(\phi_\alpha,n_\alpha)=\mu(\phi_\beta,n_\beta)$ for the solute gives rise to

$$n_\alpha = A_0 e^{g\phi_\alpha}, \quad n_\beta = A_0 e^{g\phi_\beta}. \tag{2.8}$$

The coefficient $A_0=\lambda^{-3}\exp(\mu/T-1)$ is determined from the conservation of the solute number in Eq. (2.5) as

$$A_0 = \bar{n}/\langle e^{g\phi}\rangle, \tag{2.9}$$

where $\langle\cdots\rangle$ denotes the space average in the cell. Let γ_α be the volume fraction of phase α. Neglecting the volume of the interface region, we obtain

$$\langle e^{g\phi}\rangle = \gamma_\alpha e^{g\phi_\alpha} + (1-\gamma_\alpha)e^{g\phi_\beta}. \tag{2.10}$$

From Eq. (2.5) γ_α is expressed in terms of $\bar{\phi}$ and $\bar{n}$ as

$$\gamma_\alpha = (\bar{\phi}-\phi_\beta)/\Delta\phi \tag{2.11}$$

$$= (\bar{n}-n_\beta)/\Delta n. \tag{2.12}$$

The differences between the two phases are written as

$$\Delta\phi = \phi_\alpha - \phi_\beta > 0, \quad \Delta n = n_\alpha - n_\beta > 0. \tag{2.13}$$

With the aid of Eq. (2.8), the ratio $n_\alpha/\bar{n}$ is written in terms of the compositions as

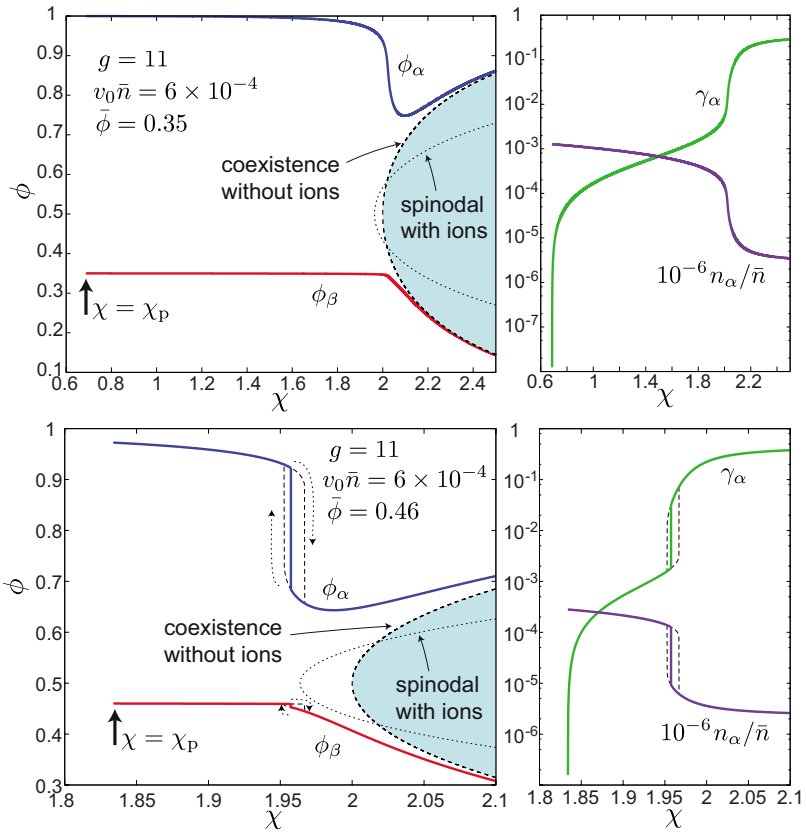

FIG. 1. (Color online) Left: compositions ϕ_α and ϕ_β vs χ. Right: semilogarithmic plots of volume fraction γ_α and normalized solute density $n_\alpha/\bar{n}$ of the water-rich phase α vs χ. Here, $\bar{n}=6\times10^{-4}v_0^{-1}$ and $g=11$. Precipitation occurs for $\chi_p<\chi\lesssim 2$. For $\bar{\phi}=0.35$ (top), ϕ_α changes continuously. For $\bar{\phi}=0.46$ (bottom), ϕ_α jumps at $\chi\cong 2$. Plotted in the left also are the coexisting region without solute (in blue) and the spinodal curve with solute [see Eqs. (3.7) and (5.2)] [23].

$$n_\alpha/\bar{n}=\Delta\phi/[(\bar{\phi}-\phi_\beta)+(\phi_\alpha-\bar{\phi})e^{-g\Delta\phi}]. \tag{2.14}$$

For not small $\Delta\phi$, we find $n_\alpha/n_\beta=e^{g\Delta\phi}\gg 1$ and $\Delta n\cong n_\alpha$. Namely, the solute density is much higher in phase α than in phase β. The solvation part $-Tgn_\alpha\phi$ of the free-energy density is significant in phase α even for small $\bar{n}$.

Next, the homogeneity relation $h(\phi_\alpha,n_\alpha)=h(\phi_\beta,n_\beta)$ for the solvent composition is written as

$$\begin{aligned} h&=f'(\phi_\alpha)-Tgn_\alpha \\ &=f'(\phi_\beta)-Tgn_\beta. \end{aligned} \tag{2.15}$$

In equilibrium, we also require minimization of the grand potential density ω defined by

$$\begin{aligned} \omega&=f_{\rm tot}-h\phi-\mu n \\ &=f-h\phi-Tn, \end{aligned} \tag{2.16}$$

where the second line follows from Eq. (2.7). In the two phases, ω assumes the same value, so that

$$f(\phi_\alpha)-f(\phi_\beta)-T\Delta n=h\Delta\phi. \tag{2.17}$$

We may derive Eqs. (2.15) and (2.17) from minimization of the total free energy F under Eq. (2.5). Using γ_α we express F as

$$F/V=\gamma_\alpha f_{\rm tot}(\phi_\alpha,n_\alpha)+(1-\gamma_\alpha)f_{\rm tot}(\phi_\beta,n_\beta), \tag{2.18}$$

where the surface free energy is neglected. If use is made of the relation $n[\ln(n\lambda^3)-g\phi]=n\ln A_0$ in the two phases, the above expression is rewritten as

$$\begin{aligned} F/V=&\gamma_\alpha f(\phi_\alpha)+(1-\gamma_\alpha)f(\phi_\beta)+T\bar{n}\ln(\bar{n}\lambda^3) \\ &-T\bar{n}\ln[\gamma_\alpha e^{g\phi_\alpha}+(1-\gamma_\alpha)e^{g\phi_\beta}]. \end{aligned} \tag{2.19}$$

The third term in the first line is a constant at constant $\bar{n}=\langle n\rangle$ and is irrelevant, but the fourth term in the second line is a singular solvation contribution at fixed $\bar{n}=\langle n\rangle$ relevant for large g (even for small $\bar{n}$). Since $\bar{\phi}=\langle\phi\rangle$ is also fixed, we should minimize

$$\tilde{\omega}=F/V-h[\gamma_\alpha\phi_\alpha+(1-\gamma_\alpha)\phi_\beta-\bar{\phi}] \tag{2.20}$$

with respect to ϕ_α, ϕ_β, and γ_α. Here, h appears as the Lagrange multiplier. With the aid of expression (2.19), the minimum conditions, $\partial\tilde{\omega}/\partial\phi_\alpha=\partial\tilde{\omega}/\partial\phi_\beta=\partial\tilde{\omega}/\partial\gamma_\alpha=0$, readily lead to Eqs. (2.15) and (2.17).

Without solute $\bar{n}=0$, two-phase coexistence is possible only for $\chi>2$. Thus, in Appendix A, we will perform the Taylor expansions of ϕ_α and ϕ_β with respect to $\bar{n}$ for $\chi>2$. We shall see that the water-rich coexistence branch is much deformed even by a very small amount of a highly preferential solute (as can be seen in Fig. 1 below).

B. Numerical results of precipitation

Next we give numerical results on the phase behavior of our system. We will set $g=11$ mostly, but will also present additional results for $g=15$ in Fig. 3. The solute density n will be measured in units of v_0^{-1}.

In Fig. 1, we display ϕ_α and ϕ_β in the left panels and n_α and γ_α in the right panels as functions of χ (or T experimentally) at $\bar{n}=6\times10^{-4}v_0^{-1}$. Due to the nonlinear solute effect, a precipitation branch appears in the range

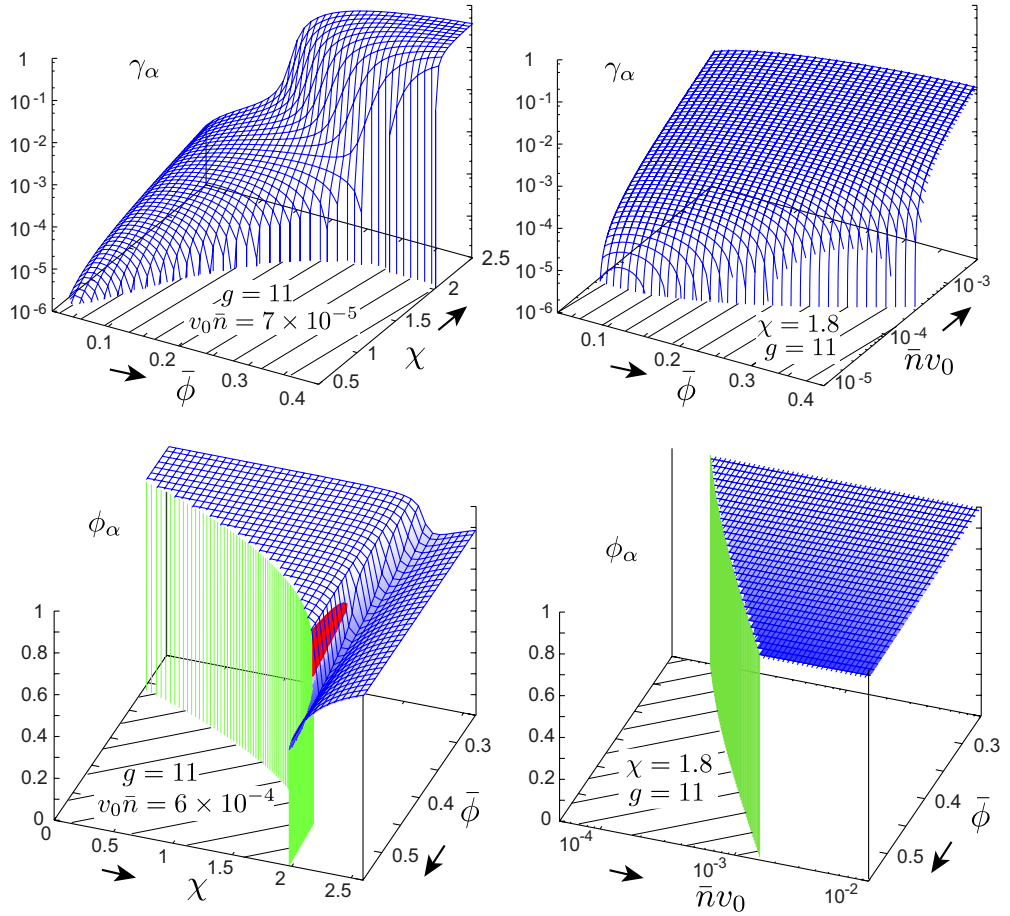

FIG. 2. (Color online) Volume fraction γ_α (top) and composition ϕ_α (bottom) of the water-rich phase α with $g=11$. Here, $\bar{n}=7\times10^{-5}$ (left top) and $\bar{n}=6\times10^{-4}$ (left bottom) in the χ-$\bar{\phi}$ plane, while $\chi=1.8$ (right) in the $\bar{n}$-$\bar{\phi}$ plane. Precipitation occurs for $\chi>\chi_{\rm p}(\bar{\phi},\bar{n})$ (left) and $\bar{n}>n_{\rm p}(\bar{\phi},\chi)$ (right) outside the slashed regions. In the left bottom, a first-order transition occurs for $\chi\cong1.95$ and $\bar{\phi}>0.395$ in a narrow perpendicular region on the surface of ϕ_α (in dark red), for which see the bottom plates in Fig. 1 also.

$$\chi_{\rm p}(\bar{\phi},\bar{n}) < \chi < 2, \tag{2.21}$$

where the solvent would be in one-phase states without solute. Here, γ_α tends to zero as $\chi\to\chi_{\rm p}$, where the lower bound $\chi_{\rm p}$ depends on $\bar{\phi}$ and $\bar{n}$. This branch appears under the condition $e^{g(1-\bar{\phi})}\gg1$ (see the next section). For large g (=11 here), the precipitated domains become solute rich (salted water for hydrophilic ions) with

$$\phi_\alpha\cong1, \quad n_\alpha\gg n_\beta=e^{-g\Delta\phi}n_\alpha. \tag{2.22}$$

The right panels are on semilogarithmic scales. With decreasing χ, we can see an increase in the solute density n_α and an decrease in the volume fraction γ_α. Details of the figure are as follows. (i) For $\bar{\phi}=0.35$ (top), ϕ_α changes rather abruptly around $\chi\sim2$ but continuously as a function of χ, being minimum at $\chi=2.05$. n_α increases up to $0.381v_0^{-1}$ as $\chi\to\chi_{\rm p}=0.687$. (ii) For $\bar{\phi}=0.46$ (bottom), the precipitation branch much shrinks with $\chi_{\rm p}=1.834$, while $n_\alpha=0.0842v_0^{-1}$ at $\chi=\chi_{\rm p}$. For this larger $\bar{\phi}$, ϕ_α changes discontinuously on a hysteresis loop in the range $1.953<\chi<1.967$. If F in Eq. (2.18) is minimized, a first-order transition is found to occur at $\chi=1.957$. Even for $\chi>2$, the two-phase coexistence is much deformed by the solute.

In Fig. 2, we show γ_α and ϕ_α in the χ-$\bar{\phi}$ plane at $\bar{n}=7\times10^{-5}$ (left top) and $\bar{n}=6\times10^{-4}$ (left bottom) and in the $\bar{n}$-$\bar{\phi}$ plane at $\chi=1.8$ (right). For fixed χ in the $\bar{n}$-$\bar{\phi}$ plane, precipitation occurs for

$$\bar{n} > n_{\rm p}(\bar{\phi},\chi), \tag{2.23}$$

where γ_α tends to zero as $\bar{n}\to n_{\rm p}$. This minimum solute density $n_{\rm p}$ depends on $\bar{\phi}$ and χ. As the crossover to the asymptotic behavior in Eq. (2.22), ϕ_α becomes appreciably smaller than 1 for $\chi\sim2$ or for $\bar{\phi}\sim0.5$. For large $\bar{\phi}\gtrsim0.5$, the precipitation branch shrinks to vanish for small solute densities, where water molecules are already abundant around solute particles in one-phase states.

In Fig. 3, at $g=11$ and 15, we show $\chi_{\rm p}(\bar{\phi},\bar{n})$ vs $\bar{\phi}$ for three values of $\bar{n}$ (left) and $n_{\rm p}(\bar{\phi},\chi)$ vs $\bar{\phi}$ for three values of χ (right). Here, $\chi_{\rm p}$ decreases with increasing $\bar{n}$ even to negative values, while $n_{\rm p}$ decreases with increasing χ. Both $\chi_{\rm p}$ and $n_{\rm p}$ decrease dramatically at small $\bar{\phi}$, and their magnitudes strongly depend on g. In fact, the curve of $\chi=\chi_{\rm p}$ sud-

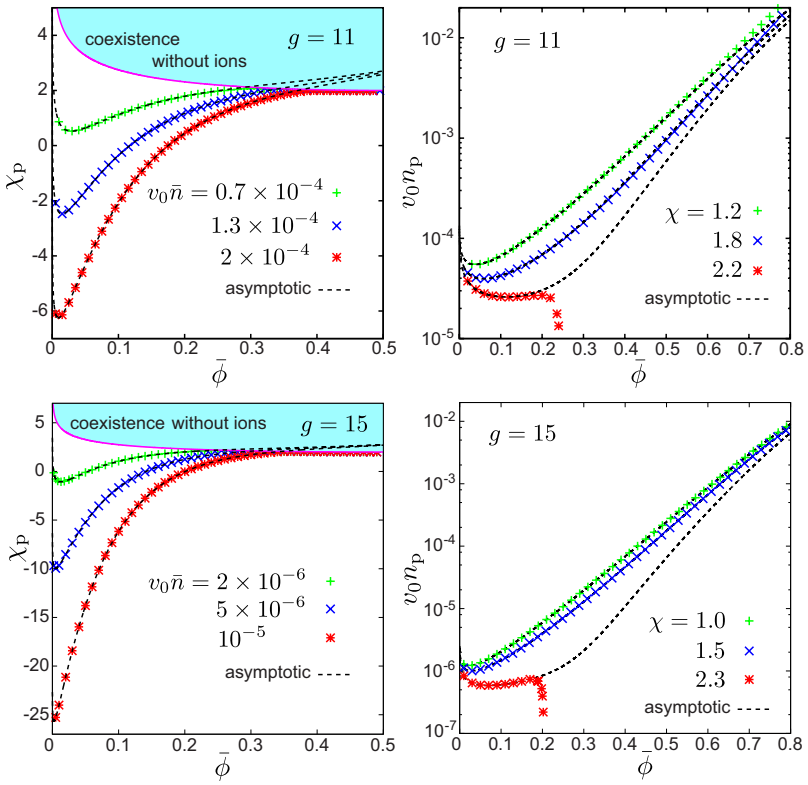

FIG. 3. (Color online) Left: $\chi_p(\bar{\phi},\bar{n})$ vs $\bar{\phi}$ for three values of $\bar{n}$ at $g=11$ (top) and 15 (bottom), which nearly coincide with the asymptotic formula (2.33) (dotted line) for $\bar{\phi}<0.35$ and converge to the coexistence curve for larger $\bar{\phi}$. Coexistence region without ions is in the upper region (in blue). Right: $v_0 n_p(\bar{\phi},\chi)$ vs $\bar{\phi}$ on a semilogarithmic scale at $g=11$ (top) and 15 (bottom). It coincides with the asymptotic formula (2.34) (dotted line) for $\chi<2$ and tends to zero at the coexistence composition 0.249 (top) or 0.204 (bottom).

denly approaches the coexistence curve with decreasing g, for example, which occurs for $g \lesssim 8$ at $\bar{n}=2\times10^{-4}$, although not shown here. Even for $\chi>2$, n_p can be calculated outside the water-rich branch of the coexistence curve, and it tends to zero as $\bar{\phi}$ approaches the coexistence composition without solute. Theoretical explanations of their behavior will be given in the following sections.

C. Theory of asymptotic behavior

We present a theory on the asymptotic behavior of the precipitation branch for $g \gg 1$ in the region $\chi<2$. At its starting point, we assume the branch satisfying Eq. (2.22) and confirm its existence self-consistently. Since $\phi_\alpha \cong 1$, the logarithmic term $[\propto(1-\phi)\ln(1-\phi)]$ in the free-energy density (2.4) is crucial in phase α.

We first neglect the term $-Tgn_\beta$ in Eq. (2.15) from $gv_0 n_\beta \ll 1$ and the term $f(\phi_\alpha)$ in Eq. (2.17) from $f(\phi_\alpha) \sim T(1-\phi_\alpha)\ln(1-\phi_\alpha)$. Note that $gv_0 n_\beta \sim 10^{-2}$ in Fig. 1. It follows a simplified equation,

$$h \cong f'(\phi_\beta) \cong -[f(\phi_\beta) + Tn_\alpha]/(1-\phi_\beta). \tag{2.24}$$

This determines the solute density n_α in phase α as a function of ϕ_β in the form

$$n_\alpha \cong G(\phi_\beta)/T, \tag{2.25}$$

where $G(\phi)$ is defined by

$$G(\phi) = -f(\phi) - (1-\phi)f'(\phi)$$
$$= -(T/v_0)[\ln\phi + \chi(1-\phi)^2]. \tag{2.26}$$

Using the free energy (2.4), we obtain the second line and plot it in the ϕ-χ plane in Fig. 4. It is positive outside the coexistence curve, ensuring $n_\alpha>0$ in Eq. (2.25).

In Eq. (2.15), we next use Eq. (2.4) for $f'(\phi_\alpha)$ to obtain

$$h \cong v_0^{-1}T[-\ln(1-\phi_\alpha) - \chi] - Tgn_\alpha \cong f'(\phi_\beta), \tag{2.27}$$

where the logarithmic term $[\propto\ln(1-\phi)]$ balances with the solvation term $(\propto gn_\alpha)$. The use of Eq. (2.25) gives

$$1-\phi_\alpha \cong A_\beta \exp[-gv_0 G(\phi_\beta)/T], \tag{2.28}$$

where the coefficient A_β is given by

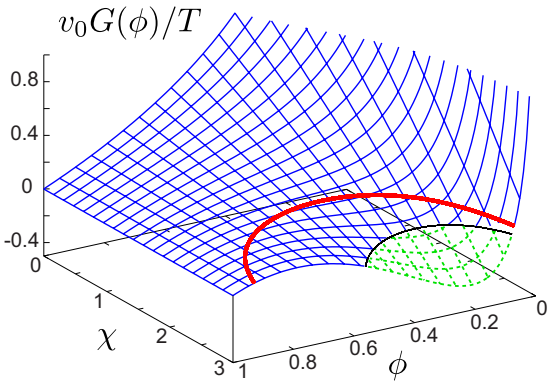

FIG. 4. (Color online) $v_0 G(\phi)/T$ defined in Eq. (2.26) in the ϕ-χ plane. It is negative only in the inner green meshed region (in broken lines), where the minimum of χ is 2.455 at $\phi=0.285$. It is positive outside it in the blue meshed region (in bold lines). The coexistence curve without solute is written on the surface (in bold red line), on which the minimum of χ is 2 at $\phi=0.5$.

$$A_\beta = \exp[-\chi - v_0 f'(\phi_\beta)/T], \tag{2.29}$$

so A_β is of order unity. The factor $\exp[-g v_0 G(\phi_\beta)/T]$ in Eq. (2.28) is very small for $g \gg 1$, leading to $\phi_\alpha \cong 1$ as in Figs. 1 and 2.

Furthermore, from Eqs. (2.12) and (2.25), the volume fraction γ_α of phase α is approximated as

$$\gamma_\alpha \cong \bar{n}/n_\alpha - e^{-g\Delta\phi} \cong T\bar{n}/G(\phi_\beta) - e^{-g\Delta\phi}. \tag{2.30}$$

The above relation is rewritten as

$$G(\phi_\beta) \cong T\bar{n}/(\gamma_\alpha + e^{-g\Delta\phi}) \cong \frac{T\bar{n}(1-\phi_\beta)}{\bar{\phi} - \phi_\beta + (1-\phi_\beta)\exp[-g(1-\phi_\beta)]}. \tag{2.31}$$

From the first to second line, we have used Eq. (2.11) and replaced $\Delta\phi$ with $1-\phi_\beta$. This equation also follows from Eqs. (2.14) and (2.25). It determines ϕ_β and $\gamma_\alpha \cong (\bar{\phi} - \phi_\beta)/(1-\phi_\beta)$. We recognize that $G(\phi_\beta)$ increases up to $T\bar{n}e^{g\Delta\phi} \cong T\bar{n}e^{g(1-\bar{\phi})}$ as $\gamma_\alpha \to 0$ or as $\phi_\beta \to \bar{\phi}$. In this limit it follows the marginal relation

$$G(\bar{\phi}) \cong T\bar{n}e^{g(1-\bar{\phi})} \quad (\gamma_\alpha \to 0). \tag{2.32}$$

If $\bar{n}$ is fixed above $n_{\rm p}$, Eq. (2.32) holds at $\chi = \chi_{\rm p}$, so that

$$\chi_{\rm p} \cong [-\ln \bar{\phi} - v_0 \bar{n} e^{g(1-\bar{\phi})}]/(1-\bar{\phi})^2, \tag{2.33}$$

where we use the second line of Eq. (2.26). Notice that the solute density $\bar{n}$ appears in the combination $\bar{n}e^{g(1-\bar{\phi})}$, and its effect of lowering $\chi_{\rm p}$ is much amplified for $g(1-\phi) \gg 1$ even for very small $\bar{n}$. [For $\bar{n}=0$ the right-hand side of Eq. (2.33) is above the coexistence curve.] On the other hand, if χ is fixed above $\chi_{\rm p}$, Eq. (2.32) holds at $\bar{n} = n_{\rm p}$. Thus, the minimum solute density $n_{\rm p}$ is estimated as

$$n_{\rm p} \cong e^{-g(1-\bar{\phi})} G(\bar{\phi})/T, \tag{2.34}$$

which is much decreased by the factor $e^{-g(1-\bar{\phi})}$.

In Fig. 3, the curves of $\chi_{\rm p}$ and $n_{\rm p}$ nearly coincide with the asymptotic formulas (2.33) and (2.34) in the range $\bar{\phi} < 0.35$ for $\chi_{\rm p}$ and in the range $\chi < 2$ for $n_{\rm p}$. They exhibit a minimum at $\bar{\phi} \sim e^{-g}/v_0 \bar{n} g$ for $\chi_{\rm p}$ and at $\bar{\phi} \sim g^{-1}$ for $n_{\rm p}$. For larger $\bar{\phi} > 0.35$, $\chi_{\rm p}$ nearly coincides with the coexistence curve, indicating disappearance of the precipitation branch. Notice that $n_{\rm p}$ decreases to zero as $\bar{\phi}$ approaches the coexistence composition $\phi_{\rm cx} = 0.249$ at $\chi = 2.2$ (top) and 0.204 at $\chi = 2.3$ (bottom), where phase separation occurs without solute.

D. Theory for small volume fraction of precipitates

We next construct an analytical theory of precipitation for small volume fraction $\gamma_\alpha \ll 1$. We will calculate F in Eq. (2.19) treating γ_α as an order parameter of the phase transition. Although this theory is applicable only for $\gamma_\alpha \ll 1$, it can yield Eq. (2.21) in the asymptotic limit.

In Eq. (2.19) we first expand ϕ_β and $f(\phi_\beta)$ with respect to γ_α as

$$\phi_\beta = (\bar{\phi} - \phi_\alpha)/(1-\gamma_\alpha) \cong \bar{\phi} + (\bar{\phi} - \phi_\alpha)\gamma_\alpha,$$

$$f(\phi_\beta) \cong f(\bar{\phi}) + f'(\bar{\phi})(\bar{\phi} - \phi_\alpha)\gamma_\alpha. \tag{2.35}$$

Let $F_0 = V f_{\rm tot}(\bar{\phi}, \bar{n})$ be the one-phase value of F (at $\gamma_\alpha = 0$). The increment $\Delta F = F - F_0$ is due to precipitate formation and is of the form

$$\Delta F/V = \Omega(\phi_\alpha)\gamma_\alpha - T\bar{n}\ln[1 + \Psi(\phi_\alpha)\gamma_\alpha], \tag{2.36}$$

where $\omega_b(\phi)$ and $\Psi(\phi)$ are defined by

$$\Omega(\phi) = f(\phi) - f(\bar{\phi}) - f'(\bar{\phi})(\phi - \bar{\phi}), \tag{2.37}$$

$$\Psi(\phi) = \exp[g(\phi - \bar{\phi})] - 1 - g(\phi - \bar{\phi}), \tag{2.38}$$

where $\bar{\phi}$ is treated as a constant, and its dependence on Ω and Φ are suppressed. In Eq. (2.36) we have not expanded the logarithmic term with respect to γ_α, because the coefficient $\Psi(\phi_\alpha)$ grows strongly as $e^{g(\phi_\alpha - \bar{\phi})}$ for $g(\phi_\alpha - \bar{\phi}) \gg 1$. (However, it will be expanded in powers of γ_α in Sec. III B.) For $\chi < 2$, the positivity $\Omega(\phi_\alpha) > 0$ follows in the region $\bar{\phi} < \phi < \phi_\alpha$ since Eq. (2.37) gives

$$\Omega(\phi_\alpha) = \int_{\bar{\phi}}^{\phi_\alpha} d\phi (\phi_\alpha - \phi) f''(\phi), \tag{2.39}$$

where $f''(\phi) = \partial^2 f/\partial^2 \phi > 0$. Note that if ϕ and $\bar{\phi}$ in $\Omega(\phi)$ are replaced with 1 and ϕ_β, respectively, $\Omega(\phi)$ becomes identical to $G(\phi_\beta)$ in Eq. (2.26). If use is made of Eq. (2.4), $\Omega(\phi)$ is explicitly written as

$$\frac{v_0}{T}\Omega(\phi) = \phi \ln\left(\frac{\phi}{\bar{\phi}}\right) + (1-\phi)\ln\left(\frac{1-\phi}{1-\bar{\phi}}\right) - \chi(\phi - \bar{\phi})^2. \tag{2.40}$$

For each given $\bar{\phi}$ and $\bar{n}$, ΔF should be minimized with respect to γ_α and ϕ_α. Here, ϕ_β is given by Eqs. (2.35). From Eq. (2.36) its derivative with respect to γ_α is

$$\frac{1}{V}\frac{\partial \Delta F}{\partial \gamma_\alpha} = \Omega(\phi_\alpha) - \frac{T\bar{n}\Psi(\phi_\alpha)}{1 + \Psi(\phi_\alpha)\gamma_\alpha}. \tag{2.41}$$

The right-hand side can vanish only when

$$Z(\phi_\alpha) \equiv \Omega(\phi_\alpha)/T\bar{n}\Psi(\phi_\alpha) < 1. \tag{2.42}$$

If $Z(\phi_\alpha) < 1$, γ_α is nonvanishing and is written as

$$\gamma_\alpha = T\bar{n}/\Omega(\phi_\alpha) - 1/\Psi(\phi_\alpha). \tag{2.43}$$

For this γ_α, ΔF in Eq. (2.36) becomes negative as

$$\Delta F/V = T\bar{n}[1 - Z(\phi_\alpha) + \ln Z(\phi_\alpha)]. \tag{2.44}$$

In the range $0 < Z < 1$, the function $1 - Z + \ln Z$ is negative and decreases with decreasing Z. In order to minimize ΔF, we should thus minimize $Z(\phi)$ or the function $\Omega(\phi)/\Psi(\phi)$ at $\phi = \phi_\alpha$. The equation to determine $\phi_\alpha = \phi_\alpha(\bar{\phi}, \chi)$ is hence given by

$$\frac{\partial}{\partial \phi_\alpha}\frac{\Omega(\phi_\alpha)}{\Psi(\phi_\alpha)} = \frac{\Omega'(\phi_\alpha)}{\Psi(\phi_\alpha)} - \frac{\Omega(\phi_\alpha)}{\Psi(\phi_\alpha)^2}\Psi'(\phi_\alpha) = 0, \tag{2.45}$$

where $\Omega'(\phi) = \partial\Omega(\phi)/\partial\phi$ and $\Psi'(\phi) = \partial\Psi(\phi)/\partial\phi$. Note that ϕ_α is independent of $\bar{n}$ for $\gamma_\alpha \ll 1$. In Fig. 5, we plot

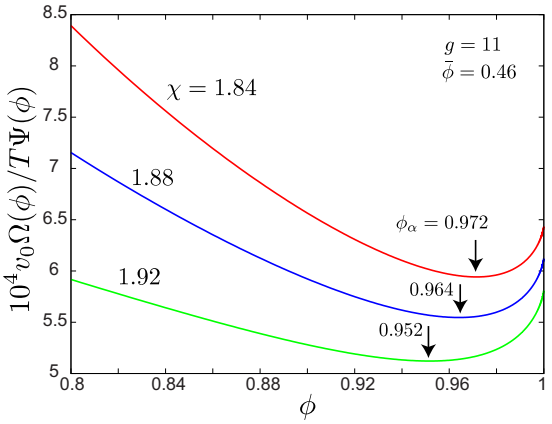

FIG. 5. (Color online) $\Omega(\phi)/\Psi(\phi)$ multiplied by $10^4 v_0/T$ for three values of χ at $g=11$ and $\bar{\phi}=0.46$. Each curve exhibits a minimum at $\phi=\phi_\alpha$, where ϕ_α is estimated as in Eq. (2.51). Each minimum value is equal to $10^4 v_0 n_p$ from Eq. (2.46).

$\Omega(\phi)/\Psi(\phi)$ for three values of χ at $\bar{\phi}=0.46$ to demonstrate the existence of its minimum at $\phi=\phi_\alpha$. In the left panel of Fig. 6, we show ϕ_α calculated from the above equation.

In terms of the above ϕ_α (dependent on $\bar{\phi}$ and χ), the minimum solute density n_p is obtained from the condition $Z(\phi_\alpha)=1$ as

$$n_p = \Omega(\phi_\alpha)/T\Psi(\phi_\alpha), \tag{2.46}$$

which is a function of $\bar{\phi}$ and χ. Then $Z(\phi_\alpha)=n_p/\bar{n}$. The condition $Z(\phi_\alpha)<1$ yields $\bar{n}>n_p$, as ought to be the case, and γ_α is also expressed as

$$\gamma_\alpha = (\bar{n}/n_p - 1)/\Psi(\phi_\alpha). \tag{2.47}$$

In the right panel of Fig. 6, we show n_p calculated from Eq. (2.46) using the data of ϕ_α in the left panel.

After ϕ_α and n_p have been determined, Eq. (2.47) indicates that an arbitrary value can be assigned to $\bar{n}$ in the range $0<\bar{n}/n_p-1\ll\Psi(\phi_\alpha)$. Furthermore, by decreasing χ at fixed $\bar{n}$ and $\bar{\phi}$, we can make $Z(\phi_\alpha)$ approach unity, where $\chi\to\chi_p=\chi_p(\bar{\phi},\bar{n})$ in Eq. (2.21). Using Eq. (2.40) we may express χ_p as

$$\chi_p = \left[\phi_\alpha \ln\frac{\phi_\alpha}{\bar{\phi}} + (1-\phi_\alpha)\ln\frac{1-\phi_\alpha}{1-\bar{\phi}}\right]/(\phi_\alpha-\bar{\phi})^2 - v_0\bar{n}\Psi(\phi_\alpha)/(\phi_\alpha-\bar{\phi})^2. \tag{2.48}$$

We notice that $(\chi-\chi_p)/(\bar{n}-n_p)=v_0\Psi(\phi_\alpha)/(\phi_\alpha-\bar{\phi})^2>0$. Relations (2.46) and (2.48) for the lower bounds are exact in our model and are consistent with the asymptotic ones (2.33) and (2.34) in the limit of $\phi_\alpha\cong 1$ and $\Psi(\phi_\alpha)\cong e^{g(1-\phi)}\gg 1$.

We now give analysis of the function $\Omega(\phi)/\Psi(\phi)$ in the range $\phi<\bar{\phi}$. If ϕ is not very close to unity, $\Omega(\phi)/\Psi(\phi)$ decreases rapidly with increasing ϕ, because $1/\Psi(\phi)\propto e^{-g\phi}$ decreases rapidly. However, as $\phi\to 1$, the logarithmic term in $f(\phi)$ eventually comes into play. To show this, we approximate $\Omega(\phi)$ for $\phi\cong 1$ as

$$\Omega(\phi) \cong G(\bar{\phi}) + \frac{T}{v_0}(1-\phi)\left[\ln\frac{1-\phi}{A_0} - 1\right], \tag{2.49}$$

where $G(\phi)$ is defined in Eq. (2.26) and $\ln(A_0)=-\chi - v_0 f'(\bar{\phi})/T$. The coefficient A_β in Eq. (2.29) tends to A_0 as $\phi_\beta\to\bar{\phi}$. The derivative of $\Omega(\phi)/\Psi(\phi)$ with respect to ϕ is thus estimated as

$$\frac{d}{d\phi}\frac{\Omega(\phi)}{\Psi(\phi)} \cong \left[-gG(\bar{\phi}) - \frac{T}{v_0}\ln\frac{1-\phi}{A_0}\right]e^{-g(\phi-\bar{\phi})}. \tag{2.50}$$

In this derivative, the logarithmic term grows weakly but can balance the solvation term ($\propto g$) as $\phi\to 1$, so that

$$1-\phi_\alpha \cong A_0 \exp[-gv_0G(\bar{\phi})/T], \tag{2.51}$$

in accord with Eq. (2.28). The asymptotic form of n_p is written as in Eq. (2.34) if we set $\Omega(\phi_\alpha)\cong G(\bar{\phi})$ and $\Psi(\phi)\cong e^{g\Delta\phi}$ in Eq. (2.46).

III. INHOMOGENEOUS COMPOSITION PROFILES

Here, still neglecting the charge effect, we examine the surface tension, the stability of a spherical droplet, and the surface adsorption near a boundary wall. These problems stem from the solvation-induced phase separation.

A. Gradient free energy and surface tension

Including the gradient free energy we assume the following simple form for the total free energy:

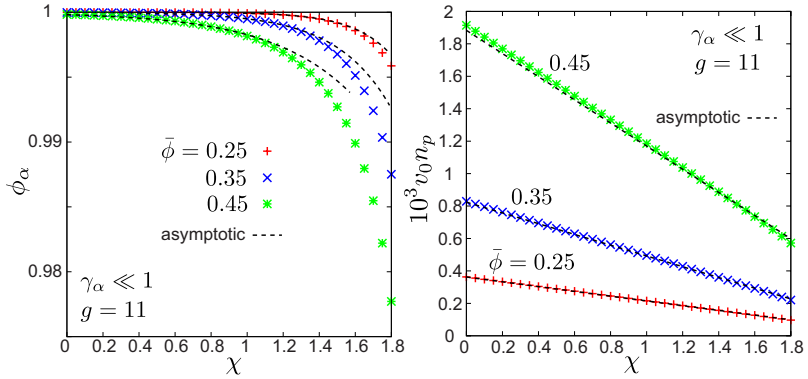

FIG. 6. (Color online) Theoretical ϕ_α in the range [0.975,1] (left) and n_p multiplied by $10^3 v_0$ (right) for $\bar{\phi}=0.25$, 0.35, and 0.45 at $g=11$. These curves are calculated for $\gamma_\alpha\ll 1$ from Eqs. (2.45) and (2.46). For these parameters, they only slightly deviate from the asymptotic formulas in Eqs. (2.34) and (2.51). The curves of n_p are nearly linear in χ from the linear dependence of $G(\bar{\phi})$ on χ.

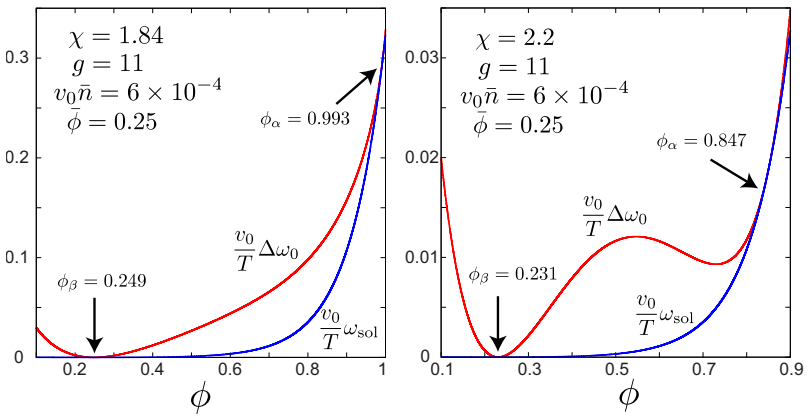

FIG. 7. (Color online) $\Delta\omega_0(\phi)$ and $\omega_{\rm sol}(\phi)$ in Eq. (3.8) in units of T/v_0 for $\chi=1.84$ (left) and 2.2 (right), where $g=11$, $\bar{\phi}=0.25$, and $v_0\bar{n}=6\times10^{-4}$. The solute part $\omega_{\rm sol}(\phi)$ is negligibly small for $\phi\lesssim0.6$ here, but it grows abruptly for larger ϕ and becomes equal to $\Delta\omega_0(\phi)$ at $\phi=\phi_\alpha$. This ensures the existence of an interface connecting phases α and β.

$$F=\int d\boldsymbol{r}\left[f_{\rm tot}(\phi,n)+\frac{C}{2}|\nabla\phi|^2\right], \tag{3.1}$$

where $f_{\rm tot}$ is given by Eq. (2.3) and C is assumed to be a positive constant. We suppose a planar interface at $z=0$ varying along the z axis and separating two phases α and β. Then $\phi=\phi(z)$ and $n=n(z)$ are functions of z with $\phi(-\infty)=\phi_\alpha$ and $\phi(\infty)=\phi_\beta$. In equilibrium, the functional derivatives of F with respect to ϕ and n are constant in space. Therefore,

$$h=\delta F/\delta\phi=f'(\phi)-Tgn-C\phi''=\text{const}, \tag{3.2}$$

where $\phi''=d^2\phi/dz^2$. Since $\mu=\delta F/\delta n=\partial f_{\rm tota}/\partial n$ is given by Eq. (2.7), the solute density depends on ϕ as

$$n(z)=A_0\exp[g\phi(z)], \tag{3.3}$$

where the coefficient A_0 is determined by Eq. (2.9) at fixed $\bar{n}=\langle n\rangle$.

We multiply Eq. (3.2) by $\phi'=d\phi/dz$ and integrate it over z to obtain

$$\Delta\omega(\phi)=\omega(\phi)-\omega(\phi_\beta)=\tfrac{1}{2}C(\phi')^2, \tag{3.4}$$

where $\omega(\phi)=f-Tn-h\phi$ is the grand potential density in Eq. (2.16) satisfying $\omega(\phi_\alpha)=\omega(\phi_\beta)$ as in Eq. (2.17). From Eq. (2.15) and the second line of Eq. (2.16), the difference $\Delta\omega(\phi)$ is written as

$$\Delta\omega(\phi)=f(\phi)-f(\phi_\beta)-f'(\phi_\beta)(\phi-\phi_\beta)-Tn_\beta[e^{g(\phi-\phi_\beta)}-g(\phi-\phi_\beta)-1]. \tag{3.5}$$

It is worth noting that the limit $\gamma_\alpha\to0$ can be attained at $\bar{n}=n_{\rm p}$. From Eq. (3.5) we find

$$\lim_{\gamma_\alpha\to0}\Delta\omega(\phi)=\Omega(\phi)-[\Omega(\phi_\alpha)/\Psi(\phi_\alpha)]\Psi(\phi), \tag{3.6}$$

where $\Omega(\phi)$ and $\Psi(\phi)$ are defined in Eqs. (2.37) and (2.38). From Eq. (2.45) the derivative of the left-hand side of Eq. (3.6) with respect to ϕ vanishes at $\phi=\phi_\alpha$. There is no singular behavior in the interface profile even in the limit $\gamma_\alpha\to0$.

The relation $\Delta\omega(\phi)\cong\omega''(\phi_\beta)(\phi-\phi_\beta)^2/2$ for $\phi\cong\phi_\beta$ follows directly from Eq. (3.5). $\Delta\omega(\phi)$ also behaves as $\omega''(\phi_\alpha)(\phi-\phi_\alpha)^2/2$ for $\phi\cong\phi_\alpha$ from Eqs. (2.15) and (2.17). Here, $\omega''(\phi)=f''(\phi)-Tg^2n(\phi)$ is the second derivative of $\Delta\omega(\phi)$ with respect to ϕ, and the correlation lengths ξ_α and ξ_β in the bulk two phases are given by

$$C\xi_\alpha^{-2}=f''(\phi_\alpha)-Tg^2n_\alpha,$$

$$C\xi_\beta^{-2}=f''(\phi_\beta)-Tg^2n_\beta, \tag{3.7}$$

in terms of which $\phi(z)-\phi_\alpha\propto e^{-|z|/\xi_\alpha}$ for $z<-\xi_\alpha$ and $\phi(z)-\phi_\beta\propto e^{-z/\xi_\beta}$ for $z>\xi_\beta$. The right-hand sides of Eqs. (3.7) should be positive for the stability of the bulk two phases. However, since $f''(\phi_\alpha)\sim T/v_0(1-\phi_\alpha)$, ξ_α becomes even shorter than $a=v_0^{1/3}$ for $\phi_\alpha\cong1$ and $C\sim T/a$. Thus, the composition varies too steeply in phase α in the present gradient theory. However, we shall see [around Eq. (3.11) below] that the surface tension is mainly determined by the composition variation in the phase β side of an interface.

In $\Delta\omega(\phi)$ in Eq. (3.5), the last term in the second line grows as $\exp[g(\phi-\phi_\beta)]$ for $\phi-\phi_\beta\gg1/g$ and can balance the other terms with increasing ϕ even for very small n_β. In Fig. 7, we illustrate this behavior by plotting the sum of the first three terms and the subtraction of the last term in the right-hand side of Eq. (3.5) separately. That is, we write $\Delta\omega(\phi)=\Delta\omega_0(\phi)-\omega_{\rm sol}(\phi)$ with

$$\Delta\omega_0(\phi)=f(\phi)-f(\phi_\beta)-f'(\phi_\beta)(\phi-\phi_\beta),$$

$$\omega_{\rm sol}(\phi)=Tn_\beta[e^{g(\phi-\phi_\beta)}-g(\phi-\phi_\beta)-1]. \tag{3.8}$$

Here, $\Delta\omega_0(\phi)$ is the grand potential difference without solute. As a function of ϕ, it increases monotonically for $\chi<2$ and exhibits positive extrema for $\chi>2$ (with ϕ_β being outside the coexistence curve).

In the Ginzburg-Landau scheme, the surface tension σ is given by the z integration of the (generalized) grand potential density $\Delta\omega(\phi)+C(\phi')^2/2$ including the gradient contribution. The use of Eq. (3.4) yields

$$\sigma=\int dzC(\phi')^2=\sqrt{CT/v_0}\int_{\phi_\beta}^{\phi_\alpha}d\phi H(\phi), \tag{3.9}$$

where we define the dimensionless function

$$H(\phi)=(2v_0/T)^{1/2}[\omega(\phi)-\omega(\phi_\beta)]^{1/2}. \tag{3.10}$$

In our theory, C is an arbitrary constant and $\sigma\propto C^{1/2}$. In Fig. 8, we plot $H(\phi)$ and $\phi(z)$ for $\chi=$(a) 1.84, (b) 1.88, and (c) 1.98 with $\bar{\phi}=0.46$ in the upper plates and for $\chi=$(d) 1.84, (e) 1.92, and (f) 2.2 with $\bar{\phi}=0.25$ in the lower plates. Here, $g=11$, $v_0\bar{n}=6\times10^{-4}$, and $C=T/a$. The values $(a^2\sigma/T,\bar{n}/n_{\rm p})$

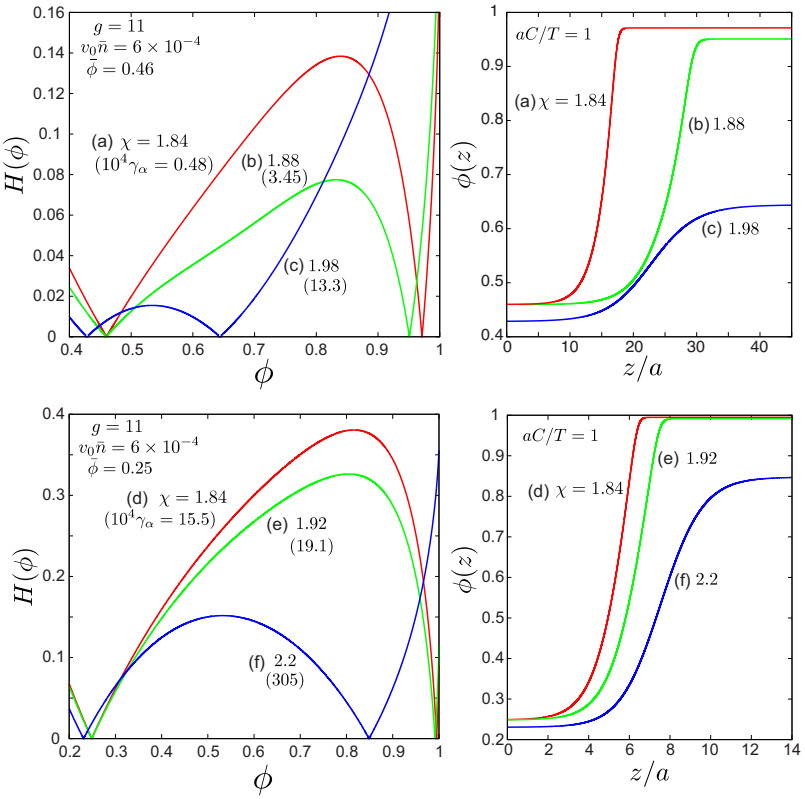

FIG. 8. (Color online) Left: $H(\phi)$ in Eq. (3.10) vs ϕ, which vanishes at $\phi=\phi_\alpha$ and ϕ_β. Right: $\phi(z)$ vs z/a, where $a=v_0^{1/3}$ and $C=T/a$. Here, $g=11$, $\bar{\phi}=0.25$, and $v_0\bar{n}=6\times10^{-4}$. In the upper plates three curves correspond to (a) $\chi=1.98$, (b) 1.88, and (c) 1.84, while in the lower plates we set (d) $\chi=2.2$, (e) 1.92, and (f) 1.84. In the parentheses the volume fraction γ_α multiplied by 10^4 is written for each curve (left).

in these cases are (a) (0.044,1.01), (b) (0.024,1.17), (c) (0.0021,2.25), (d) (0.19,6.6), (e) (0.16,7.7), and (f) (0.064,∞). In case (c), the system is close to the solvent criticality and ξ_β is relatively long. In case (f), $\bar{\phi}$ is slightly larger than the composition 0.249 on the oil-rich branch of the coexistence curve without solute, so phase separation occurs even without solute or $n_p=0$. The shape of $H(\phi)$ in Fig. 8 is roughly triangular except case (f), so we obtain a simple estimate,

$$\sigma \sim C(\Delta\phi)^2/\xi_\beta. \tag{3.11}$$

Since ξ_α is considerably shorter than ξ_β, we may approximate the interface profile as

$$\phi(z) - \phi_\beta \sim \Delta\phi \exp(-z/\xi_\beta), \tag{3.12}$$

in the region $0<z\lesssim\xi_\beta$, neglecting the variation in the region $-\xi_\alpha\lesssim z<0$. Substitution of Eq. (3.12) into Eq. (3.9) yields Eq. (3.11). Behaviors (3.11) and (3.12) hold even in the limit $\gamma_\alpha\to0$.

B. Discontinuous appearance of a droplet due to surface tension: Minimum droplet radius R_m

As an example, we suppose a single spherical droplet of phase α suspended in phase β in equilibrium, accounting for the effect of the surface tension σ. The droplet radius R is so small that the following condition holds:

$$u \equiv \Psi(\phi_\alpha)\gamma_\alpha \ll 1, \tag{3.13}$$

where $\gamma_\alpha=4\pi R^3/3V$ and $\Psi(\phi_\alpha)\sim e^{g(1-\bar{\phi})}$. We add the surface free energy $4\pi\sigma R^2$ to ΔF in Eq. (2.36) and expand the logarithmic factor there as $\ln(1+u)\cong u-u^2/2$. The resultant total free energy reads

$$\Delta F_{\rm tot} = V\left(-w\gamma_\alpha + \tfrac{1}{2}T\bar{n}u^2\right) + 4\pi\sigma R^2, \tag{3.14}$$

up to second order in γ_α. The coefficient w is defined by

$$w = -\Omega(\phi_\alpha) + T\bar{n}\Psi(\phi_\alpha) \tag{3.15}$$

$$= \Omega(\phi_\alpha)(\bar{n}/n_p - 1) \tag{3.16}$$

$$= Tv_0^{-1}(\phi_\alpha - \bar{\phi})^2(\chi - \chi_p), \tag{3.17}$$

where n_p in the second line is the minimum solute density in Eq. (2.46) and χ_p in the third line is the minimum interaction parameter in Eq. (2.48). A droplet can exist only for $w>0$, which means $\bar{n}>n_p$ or $\chi>\chi_p$. It is convenient to introduce two characteristic lengths by

$$R_c = 2\sigma/w, \tag{3.18}$$

$$R_m = (3\sigma V/2\pi T\bar{n})^{1/4}\Psi(\phi_\alpha)^{-1/2}, \tag{3.19}$$

in terms of which $\Delta F_{\rm tot}$ in Eq. (3.14) is rewritten as

$$\Delta F_{\rm tot}/4\pi\sigma = R^2 - 2R^3/3R_c + R^6/3R_m^4. \tag{3.20}$$

For $\sigma\sim T/a^2$ we roughly estimate

$$R_c \sim a/(\bar{n}/n_p - 1) \sim a/(\chi - \chi_p),$$

$$R_m \sim (n_p/\bar{n})^{1/4}(Va)^{1/4}e^{-g(1-\bar{\phi})/4}. \tag{3.21}$$

If $\bar{n}$ (or χ) is increased above n_p (or χ_p), R_m soon exceeds R_c for large V, despite the reducing factor $e^{-g(1-\bar{\phi})/4}$.

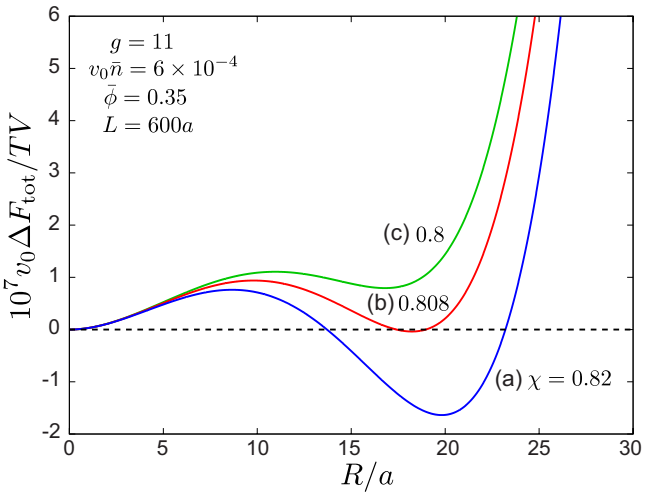

FIG. 9. (Color online) $\Delta F_{\rm tot}$ including the surface free energy vs R/a for (a) χ=0.82, (b) 0.808, and (c) 0.8 from below. At the minimum with positive R, the droplet is stable for (a), marginal for (b), and metastable for (c), while $\bar{n}/n_{\rm p}$=1.080 for (a), 1.073 for (b), and 1.067 for (c). Here, R=18.23a at the minimum for (b).

We should minimize $\Delta F_{\rm tot}$ in Eq. (3.20) as a function of R. For $R>0$ we require $\Delta F_{\rm tot}<0$ and $\partial \Delta F_{\rm tot}/\partial R=0$. The latter condition is written as

$$1 - R/R_c + R^4/R_{\rm m}^4 = 0, \tag{3.22}$$

under which $\Delta F_{\rm tot}=4\pi R^2(2-R/R_c)/3<0$, so $R>2R_c$ is needed. This inequality can be satisfied only for

$$R_c < R_{\rm m}/2 \quad \text{or} \quad w > 4\sigma/R_{\rm m}, \tag{3.23}$$

which will be evident in Fig. 18. If the above condition is not satisfied, there is no equilibrium droplet. As $R_{\rm m}/R_c \to 2$, we have $R \to R_{\rm m}$. Here, u in Eq. (3.13) is of order $(n_{\rm p}/\bar{n})^{3/4}[a^3 e^{g(1-\bar{\phi})}/V]^{1/4}$ and can be much smaller than unity for large V. Thus, $R_{\rm m}$ is the minimum equilibrium droplet radius in the presence of the surface tension. For $R_{\rm m}/R_c \gg 1$, the surface free energy becomes negligible and

$$R \cong (R_{\rm m}^4/R_c)^{1/3} = [3Vw/4\pi\bar{n}\Psi(\phi_\alpha)^2]^{1/3}. \tag{3.24}$$

We also note that the transition occurs for $\bar{n}/n_{\rm p}-1 \gtrsim a/R_{\rm m}$ from Eq. (3.16) or for $(1-\bar{\phi})^2(\chi-\chi_{\rm p}) \gtrsim a/R_{\rm m}$ from Eq. (3.17).

In Fig. 9, we plot $\Delta F_{\rm tot}=\Delta F+4\pi\sigma R^2$ as a function of R in the spherically symmetric geometry, where $\bar{\phi}$=0.35, $v_0\bar{n}$=6 $\times 10^{-6}$, and g=11. The cell volume is $V=4\pi L^3/3 \cong 0.9 \times 10^9 v_0$ with L=600a. Here, we use Eq. (2.36) for ΔF and not the expansion form of ΔF in Eq. (3.14). For the three curves in Fig. 9, the parameter u in Eq. (3.13) is surely smaller than unity and Eq. (3.14) or Eq. (3.20) is a good approximation. In fact, at the minimum position of curve (b) in Fig. 9, we have R=18.23a, σ=0.231T/a^2, and Ω =0.706T/v_0, while $R_{\rm m}$=17.89a from Eqs. (3.20) and (3.22) in this case. In the next section, we will present simulation results in the same situation for hydrophilic ions.

C. Solvation-induced prewetting transition

We note that Eq. (3.4) can also be used to examine the composition profile $\phi(z)$ near a boundary wall at z=0. Here, slightly below the precipitation curve $\chi=\chi_{\rm p}$ (or $\bar{n}=n_{\rm p}$), we may predict a first-order prewetting transition [33,34] at χ $=\chi_{\rm tr}(<\chi_p)$ with increasing χ, where the surface adsorption changes discontinuously. This result is related to the experiment by Beaglehole [21].

Far from the wall, we assume that $\phi(z)$ and $n(z)$ tend to $\bar{\phi}$ and $\bar{n}$, respectively. Then Eq. (3.4) holds with

$$\Delta\omega(\phi) = \Omega(\phi) - T\bar{n}\Phi(\phi), \tag{3.25}$$

where $\Omega(\phi)$ and $\Phi(\phi)$ are defined by Eqs. (2.37) and (2.38). The previous $\Delta\omega(\phi)$ in Eqs. (3.4) and (3.5) becomes the above $\Delta\omega(\phi)$ if ϕ_β and n_β there are replaced with $\bar{\phi}$ and $\bar{n}$, respectively. Below the precipitation curve $\chi=\chi_{\rm p}$, $\Delta\omega(\phi)$ is positive for $\phi>\bar{\phi}$ and again approaches zero at $\phi \cong \phi_\alpha$ as $\chi \to \chi_{\rm p}$. See Fig. 7 for its behavior. Assuming $\phi'(z)$ $=d\phi(z)/dz<0$, we rewrite Eq. (3.4) as

$$\frac{d\phi}{dz} = -\sqrt{2\Delta\omega(\phi)/C}. \tag{3.26}$$

In addition to the bulk free energy F in Eq. (3.1), we assume the surface free energy

$$F_s = -\int dS\alpha_{\rm w}\phi = -S\alpha_{\rm w}\phi_s, \tag{3.27}$$

where $\int dS$ is the surface integral at z=0, S is the surface area, $\phi_s=\phi(0)$, and α_w is a parameter arising from the short-range interaction between the solvent and the surface. Here, $\alpha_w>0$ if the boundary wall is hydrophilic and the solute is hydrophilic. The boundary condition of $\phi(z)$ at z=is given by

$$C\phi'(0) = -\alpha_{\rm w}. \tag{3.28}$$

Then $\sqrt{2C\Delta\omega(\phi)}=\alpha_{\rm w}$ at $\phi=\phi_s$. The surface free-energy density per unit area is then written as [33,34]

$$\mathcal{F}_{\rm ad} = \int_0^\infty dz[\Omega(\phi) - T\bar{n}\Psi(\phi)] - \alpha_{\rm w}\phi_s$$
$$= \int_{\bar{\phi}}^{\phi_s} d\phi[\sqrt{2C\Delta\omega(\phi)} - \alpha_{\rm w}] - \alpha_{\rm w}\bar{\phi}. \tag{3.29}$$

Without solute, the composition increases by $\alpha_w\xi/C$ on the surface for $|\alpha_w| \ll T/a^2$, where ξ is the correlation length. However, in the presence of solute with $g \gg 1$, the adsorption on the surface can be strong with ϕ_s close to unity for $g\alpha_w\xi/C \gtrsim 1$ even when $\bar{n}$ is very small. In such cases, $w_{\rm sol}$ and Δw_0 in Eq. (3.8) are of the same order on the surface (see Fig. 7). In the left panel of Fig. 10, $\sqrt{2v_0\Delta\omega(\phi)/T}$ vs ϕ is displayed for $\chi=\chi_{\rm tr}$=1.885 and $\chi_{\rm p}$=1.8997, where $\bar{\phi}$ =0.36, $\bar{n}=2\times10^{-4}$, and $\alpha_{\rm w}=0.165(CT/v_0)^{1/2}$. It demonstrates the presence of a first-order prewetting transition. In the right panel of Fig. 10, the composition profile $\phi(z)$ is shown slightly before and after the transition.

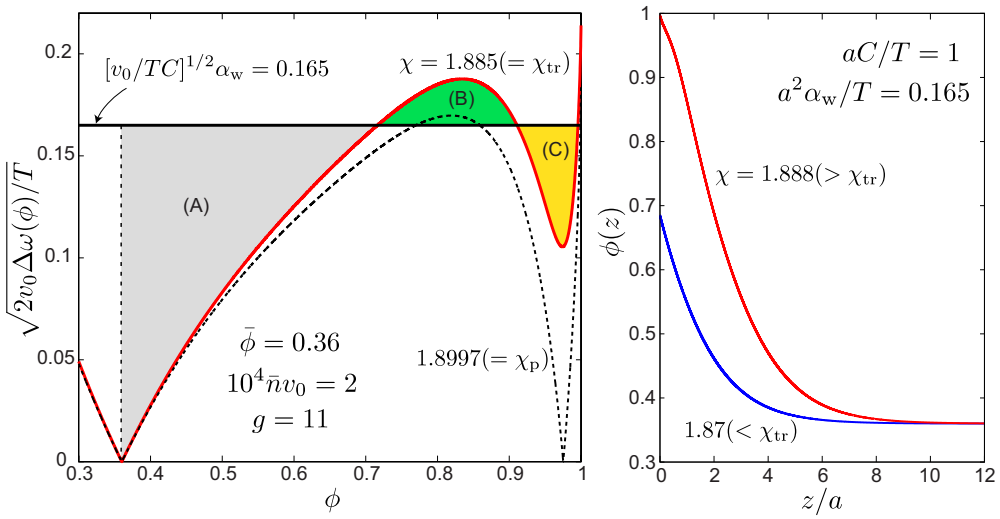

FIG. 10. (Color online) Left: $\sqrt{2v_0\Delta\omega(\phi)/T}$ vs ϕ with $\bar{\phi}=0.36$ and $v_0\bar{n}=2\times10^{-4}$, where $\Delta\omega(\phi)$ is defined in Eq. (3.25). For $\alpha_w=0.165(CT/v_0)^{1/2}$, a first-order prewetting transition at a wall occurs at $\chi=\chi_{tr}=1.885$, where areas (B) and (C) coincide. Bulk two-phase coexistence is realized for $\chi>\chi_p=1.8997$. Right: $\phi(z)$ for $C=T/a$ near the wall before and after the prewetting transition.

IV. HYDROPHILIC SALT

We now treat aqueous mixtures containing a small amount of hydrophilic monovalent salt. We shall see that the charge imbalance appears only near the interface as an electric double layer. In the statics of the present problem, the role of the electrostatic interaction is thus to shift the surface tension slightly (see the last paragraph of Sec. IV A) [23]. In the dynamics, on the other hand, electric double layers around the droplet surfaces should suppress fusion of approaching droplets. Such dynamical aspects are beyond the scope of this paper and should be studied in the future.

A. Preferential ion solvation

We write the cation density as n_1 and the anion density as n_2. Their total amounts are fixed as

$$\int d\boldsymbol{r} n_1 = \int d\boldsymbol{r} n_2 = V\bar{n}/2. \tag{4.1}$$

These densities both tend to $n_\alpha/2$ or $n_\beta/2$ in the bulk regions of phase α or β due to the charge balance. The electric charge density $e(n_1-n_2)$ gives rise to the electric potential Φ satisfying the Poisson equation

$$\nabla\cdot\varepsilon\nabla\Phi = -4\pi e(n_1-n_2). \tag{4.2}$$

The dielectric constant $\varepsilon(\phi)$ can depend on ϕ and has been assumed to be of the form

$$\varepsilon(\phi) = \varepsilon_0 + \varepsilon_1\phi. \tag{4.3}$$

Neglecting the image interaction [23,35], we assume the total free energy F in the following form [23]:

$$F = \int d\boldsymbol{r}\left[f(\phi) + \frac{1}{2}C|\nabla\phi|^2 + \frac{\varepsilon}{8\pi}|\nabla\Phi|^2 + T\sum_{i=1,2}[n_i\ln(n_i\lambda_i^3) - g_i\phi n_i]\right], \tag{4.4}$$

where the third term is the electrostatic contribution and the terms proportional to g_i represent the solvation interaction among the ions and the solvent composition. λ_1 and λ_2 are the thermal de Broglie lengths of the two ion species.

Let us explain the solvation terms in more detail. The ion chemical potentials due to solvation in aqueous mixtures strongly depend on the ambient solvent composition ϕ [23,36]. We write them as $\mu^i_{sol}(\phi)$, where i represents the ion species. We assume the linear form

$$\mu^i_{sol}(\phi) = \mu^i_0 - Tg_i\phi, \tag{4.5}$$

where the first terms are irrelevant constants. This linear dependence is adopted to gain the physical consequences in the simplest manner and should not be taken too seriously [37]. In aqueous solutions, $g_i>0$ for hydrophilic ions and $g_i<0$ for hydrophobic ions. When two phases α and β coexist, the difference

$$\Delta\mu^i_{sol} = \mu^i_{sol}(\phi_\beta) - \mu^i_{sol}(\phi_\alpha) \tag{4.6}$$

is called the Gibbs transfer free energy in electrochemistry (usually measured in units of kJ/mol), leading to an electric potential difference across an interface, called the Galvani potential difference. If we assume linear form (4.5), it is expressed as

$$\Delta\mu^i_{sol} = Tg_i\Delta\phi. \tag{4.7}$$

For example, in water-nitrobenzene (NB) at 300 K, it can be estimated as $17T$ for Na^+ and as $19T$ for Cl^- per ion. In this mixture, the two phases are strongly segregated (where the water content is 0.168 M in the NB-rich phase), so we have $\Delta\phi\cong1$ and find $g_i=15-20$ for small hydrophilic monovalent

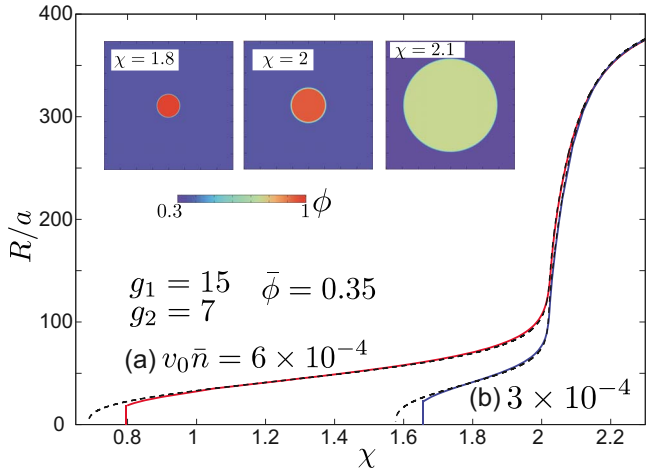

FIG. 11. (Color online) R/a vs χ (bold line) with hydrophilic ions calculated from the free energy (4.4) for (a) $v_0\bar{n}=3\times10^{-4}$ (right blue line) and (b) 6×10^{-4} (left red line). Plotted also are theoretical curves from the approximate free energy (2.36) without the surface free energy (dotted line). Inset: shapes of a spherical water-rich droplet in equilibrium for $\chi=1.8$, 2.0, and 2.1 at $v_0\bar{n}=6\times10^{-4}$, in the region $-400<x$, $y<400$, $z=0$, where the colors represent the water composition according to the color bar.

ions. In heavy water-3MP, the selective solvation has been found to induce mesoscopic phases with periodic structures for antagonistic salt. The Gibbs transfer free energies of hydrophilic ions for water-3MP should not be larger than or at least of the same order as those for water-NB, in view of the fact that the dielectric constants of 3MP and NB are 9 and 35, respectively.

We may calculate the composition and ion profiles from the homogeneity of the chemical potentials $h=\delta F/\delta\phi$ and $\mu_i=\delta F/\delta n_i$, where

$$h = f' - C\nabla^2\phi - \frac{\varepsilon_1}{8\pi}|\nabla\Phi|^2 - \sum_i g_i n_i. \tag{4.8}$$

If μ_i are homogeneous, we obtain the modified Poisson-Boltzmann relations

$$n_i = \tfrac{1}{2}n_\beta \exp[g_i(\phi-\phi_\beta) \mp e(\Phi-\Phi_\beta)/T], \tag{4.9}$$

where $-$ is for $i=1$ and $+$ is for $i=2$. The potential Φ tends to constants Φ_α and Φ_β in the bulk regions. From the charge neutrality in the bulk regions, the potential difference between the two phases is given by

$$\Delta\Phi = \Phi_\alpha - \Phi_\beta = T(g_1-g_2)\Delta\phi/2e. \tag{4.10}$$

Then the ion densities in the two phases satisfy

$$n_\alpha/n_\beta = \exp[(g_1+g_2)\Delta\phi/2]. \tag{4.11}$$

The charge density appears only near the interface for $g_1\neq g_2$ forming an electric double layer (see Fig. 11). As a result, the bulk phase relations in Eqs. (2.8)–(2.18) for neutral particles still hold for ions with the correspondence relations

$$n = n_1 + n_2, \quad g = (g_1+g_2)/2. \tag{4.12}$$

For $g_1=g_2$ we have $n_1=n_2=n/2$.

The thickness of the electric double layer is on the order of the Debye screening length, λ_α in the phase α side and λ_β in the phase β side, where

$$\lambda_K = (\varepsilon_K T/4\pi n_K e^2)^{1/2}, \tag{4.13}$$

where $K=\alpha$ or β. For hydrophilic ions, $\lambda_\alpha \ll \lambda_\beta$ holds from $n_\alpha \gg n_\beta$ and λ_α is longer than the interface thickness except close to the solvent criticality. We assume that the domain size is much longer than λ_β.

We found that the surface tension of an interface of a precipitated domain is slightly decreased by the electric double layer appearing for $g_1\neq g_2$. In fact, for $v_0\bar{n}\sim10^{-3}$, it is smaller by a few percent for $g_1=15$ and $g_2=7$ than for $g_1=g_2=11$, where the other parameters are common.

B. Proposed experiment: A single droplet

We performed simulation of a single water-rich droplet in the presence of hydrophilic ions. We have already presented a theory for neutral solute in the same situation in Sec. III B. Experimentally, we may also suppose a collection of monodisperse droplets much separated from one another, where the volume per droplet (the inverse of the droplet density) should be treated as the system volume V.

The simulation details are as follows. We calculated equilibrium profiles of $\phi(r)$ and $n_i(r)$ by minimizing F in Eq. (4.3) around a spherical water-rich droplet with radius R in a spherical cell with radius $L=600a$. At $\bar{\phi}=0.35$, we set $\bar{n}$ =(a) 6×10^{-4} or (b) 3×10^{-4}. The other parameters are $g_1=15$, $g_2=7$, $C=T/a$, and $e^2/T=120a$. The dielectric constant depends on ϕ as $\varepsilon=40(1+\phi)$. Since $g_1>g_2$, an electric double layer is produced at the interface here.

In Fig. 11, we show the equilibrium R vs χ together with shapes of the droplet for three values of χ. The droplet disappears due to the surface tension at $R=18.52a$ and $\chi=0.799$ for (a) and $R=22.18a$ and $\chi=1.656$ for (b). The corresponding value of $\bar{n}/n_p$ is 1.067 for (a) and 1.102 for (b). These curves are close to those calculated from the approximate free energy (2.36) before the droplet disappearance. The characteristic features can also be calculated from the more approximate free energy (3.14) or (3.20).

In Fig. 12, the profiles of the potential $\Phi(r)$ and the ion densities $n_1(r)$ and $n_2(r)$ are presented for $\chi=1.7$ in case (a), which follow from Eqs. (3.2) and (3.7). Here, $\phi_\alpha=0.993$ and $n_\alpha=0.352v_0^{-1}$ within the droplet and $\phi_\beta=0.349$ and $n_\beta=2.55\times10^{-4}v_0^{-1}$ outside it. The potential $\Phi(r)$ relaxes with the Debye length $\lambda_\beta=11.8a$ and is well fitted to the one-dimensional solution of the nonlinear Poisson-Boltzmann equation (dotted line). In Fig. 13, the equilibrium R is displayed as a function of χ for $v_0\bar{n}=$(a) 6×10^{-4} and (b) 3×10^{-4}. Remarkably, the droplet disappeared at $R=18.52a$ and $\chi=0.799$ for (a) and at $R=22.18a$ and $\chi=1.656$ for (b) due to the surface tension effect. This critical radius for curve (a) nearly coincides with the droplet radius $R=18.23a$ at the minimum of the curve (b) in Fig. 9. We recognize that the relations of R vs χ here are little affected by the electric

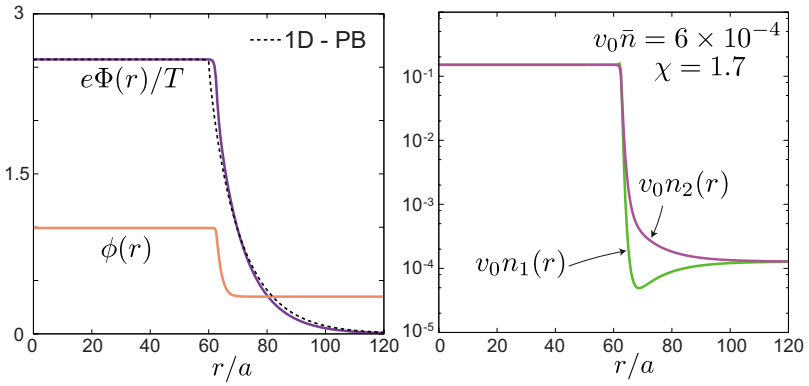

FIG. 12. (Color online) Normalized potential $e\Phi(r)/T$ (with $\Phi_\beta=0$) and water volume fraction $\phi(r)$ (left). Normalized ion densities $v_0 n_1(r)$ and $v_0 n_2(r)$ (right). Here, $\chi=1.7$ and $e\Delta\Phi=3T$. The other parameters are the same as in Fig. 11. In the phase β region near the interface, $\Phi(r)$ well agrees with the one-dimensional solution of the nonlinear Poisson-Boltzmann equation (dotted line) and there appears an electric double layer due to nonvanishing n_1-n_2.

double layer. Hence, they are close to those of neutral solvent with $g=11$ for the same $\bar{\phi}$ and $\bar{n}$.

V. HOMOGENEOUS NUCLEATION FROM ONE-PHASE STATES

We start with homogeneous one-phase states without impurities (other than the solute or the salt under consideration). We assume that the boundary walls are hydrophobic and formation of a water-rich wetting layer is suppressed. In this situation, the precipitation predicted in this paper can be realized via homogeneous nucleation for $\bar{n}>n_{\rm p}$ or $\chi>\chi_{\rm p}$. Therefore, we calculate the nucleation rate in the initial stage of nucleation. It is not much affected by the electrostatic interaction for hydrophilic ions, and we treat a neutral solute in the following. We also neglect temperature inhomogeneity and treat χ as a homogeneous constant.

It is worth noting that water droplets can easily be produced around hydrophilic ions in metastable gas mixtures containing water vapor. Here, ions play the role of nucleation seeds on which hydration-induced condensation is favored. A Ginzburg-Landau approach to this problem was also presented [38].

A. Linear stability and metastability

We first examine the linear stability of a one-phase state with $\langle\phi\rangle=\bar{\phi}$ and $\langle n\rangle=\bar{n}$. If $f_{\rm tot}$ in Eq. (2.3) is expanded with respect to the deviations $\delta\phi=\phi-\bar{\phi}$ and $\delta n=n-\bar{n}$, the second-order free-energy deviation is written as

$$(\delta f_{\rm tot})_2=\frac{1}{2}f''(\bar{\phi})(\delta\phi)^2-Tg\,\delta\phi\delta n+\frac{T}{2\bar{n}}(\delta n)^2. \quad (5.1)$$

If the right-hand side is non-negative definite, the one-phase state is stable or metastable. Minimization with respect to δn is achieved at $\delta n=g\bar{n}\delta\phi$, leading to $(\delta f_{\rm tot})_2=[f''(\bar{\phi})-T\bar{n}g^2](\delta\phi)^2/2$. Thus, the spinodal curve is expressed as

$$f''(\bar{\phi})-T\bar{n}g^2=0. \quad (5.2)$$

See the left panels in Fig. 1 for this spinodal curve. One-phase states are linearly stable outside this curve.

In the presence of the Coulomb interaction, the spinodal curve is still given by Eq. (5.2) with the replacement $g=(g_1+g_2)/2$ in Eq. (4.12) under the condition $\gamma_{\rm p}<1$. Here, $\gamma_{\rm p}$ is a parameter representing the degree of solvation asymmetry between the cations and anions (which should not be confused with the volume fraction γ_α of phase α). For monovalent ions it is given by

$$\gamma_{\rm p}=(T/16\pi C)^{1/2}|g_1-g_2|. \quad (5.3)$$

For most hydrophilic ion pairs, we should have $\gamma_{\rm p}<1$. On the other hand, the reverse condition $\gamma_{\rm p}>1$ can be realized for antagonistic salt composed of hydrophilic and hydrophobic ion pairs [13,22,23]. Addition of such a salt leads to a decrease in the surface tension and mesophases formation. In this paper, we consider hydrophilic ions with $\gamma_{\rm p}<1$ for simplicity.

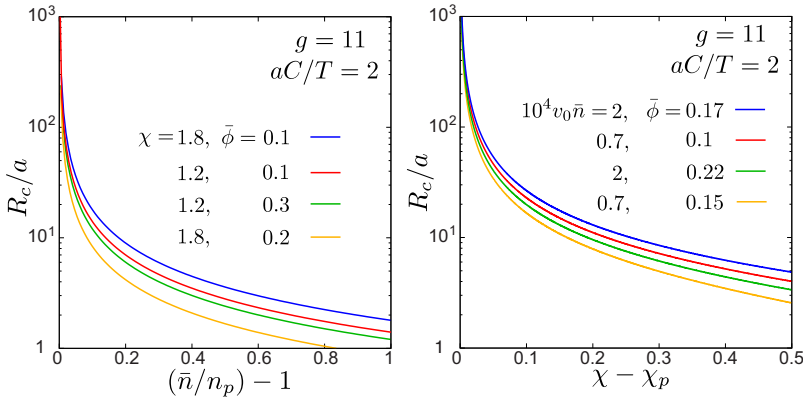

FIG. 13. (Color online) Critical radius R_c in Eq. (3.18) as a function of $\bar{n}/n_{\rm p}-1$ for $(\chi,\bar{\phi})=(1.8,0.1)$, $(1.2,0.1)$, $(1.2,0.3)$, and $(1.8,0.2)$ from above (left) and as a function of $\chi-\chi_{\rm p}$ for $(10^4 v_0\bar{n},\bar{\phi})=(2,0.17)$, $(0.7,0.1)$, $(2,0.22)$, and $(0.7,0.15)$ from above (right). Here, $g=11$ and $C=2T/a$.

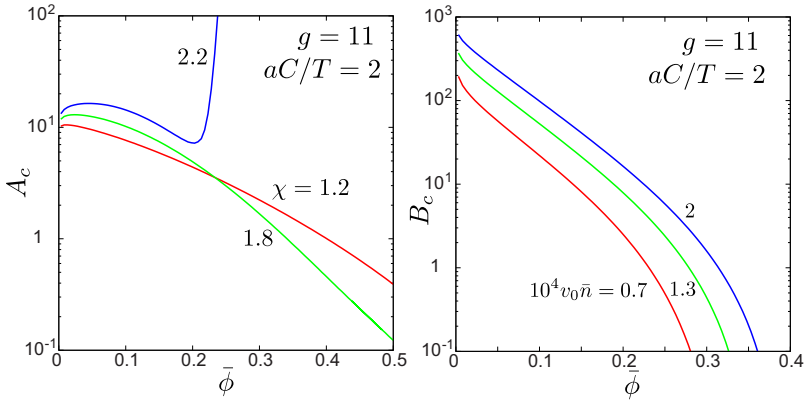

FIG. 14. (Color online) A_c at fixed χ in Eq. (5.11) (left) and B_c at fixed $\bar{n}$ in Eq. (5.12) (right) as functions of $\bar{\phi}$ for $g=11$ and $C=2T/a$. For $\chi > 2$ (left), there is no barrier or $A_c \to \infty$ as $\bar{\phi}$ approaches the equilibrium coexistence composition.

B. Droplet free energy and nucleation rate

In the early stage of nucleation, the volume fraction γ_α of the new phase is very small and the droplets may be treated independently. Hence, we consider a single droplet with radius R in the classical nucleation theory [32]. The composition and the solute density far from the droplet are $\bar{\phi}$ and $\bar{n}$. A key quantity here is the free energy $\Delta F(R)$ needed to create a droplet of the new phase.

To derive $\Delta F(R)$, we use the total free-energy density $f_{\rm tot}(\phi,n)$ in Eq. (2.3). It is equal to $\bar{f}_{\rm tot}=f_{\rm tot}(\bar{\phi},\bar{n})$ in the initial homogeneous state and remains so far from the droplet, while it is equal to $f^\alpha_{\rm tot}=f_{\rm tot}(\phi_\alpha,n_\alpha)$ inside the droplet. Here, ϕ_α and n_α are the composition and the solute density inside the droplet, respectively. The change in the total free energy is

$$\Delta F(R) = \frac{4\pi}{3}R^3[f^\alpha_{\rm tot} - \bar{f}_{\rm tot}] + \int_{r>R} d\boldsymbol{r}[f_{\rm tot}(\phi,n) - \bar{f}_{\rm tot}] + 4\pi\sigma R^2. \tag{5.4}$$

In the right-hand side, the first term is the contribution from the droplet interior, the second term is that of the droplet exterior, and the last term is the surface tension term. Outside the droplet we assume small deviations of ϕ and n from the initial values $\bar{\phi}$ and $\bar{n}$, so that we set $f_{\rm tot}(\phi,n)-\bar{f}_{\rm tot}=\bar{h}(\phi-\bar{\phi})+\bar{\mu}(n-\bar{n})$, where $\bar{h}$ and $\bar{\mu}$ are the values of h in Eq. (2.6) and μ in Eq. (2.7) in the initial metastable state. Further we note that the integrals of $\phi-\bar{\phi}$ and $n-\bar{n}$ in the whole space vanish from the conservation relations (2.5), so that their space integrals outside the droplet are equal to $-(4\pi/3)R^3(\phi_\alpha-\bar{\phi})$ and $-(4\pi/3)R^3(n_\alpha-\bar{n})$, respectively. Therefore, it follows the standard form [32]

$$\Delta F(R) = -\frac{4\pi}{3}R^3 w + 4\pi R^2\sigma. \tag{5.5}$$

The coefficient w represents the degree of metastability and is of the form

$$\begin{aligned} -w &= f^\alpha_{\rm tot} - \bar{f}_{\rm tot} - \bar{h}(\phi_\alpha - \bar{\phi}) - \bar{\mu}(n_\alpha - \bar{n}) \\ &= \Omega(\phi_\alpha) - T\bar{n}\Psi(\phi_\alpha), \end{aligned} \tag{5.6}$$

where $\Omega(\phi_\alpha)$ and $\Psi(\phi_\alpha)$ are given in Eqs. (2.37) and (2.38). From the second line of Eq. (5.6), this w coincides with w introduced in Eq. (3.15). It is proportional to $\bar{n}-n_{\rm p}$ and $\chi-\chi_{\rm p}$ as in Eqs. (3.16) and (3.17), where $n_{\rm p}$ and $\chi_{\rm p}$ are defined in Eqs. (2.46) and (2.48).

The critical radius is $R_c=2\sigma/w$ as in Eq. (3.18). At $R=R_c$, $\Delta F(R)$ attains a maximum given by

$$F_c = 16\pi\sigma^3/3w^2. \tag{5.7}$$

In the classical nucleation theory, critical droplets appear with a constant rate I per unit time and per unit volume. It is called the nucleation rate and is of the form

$$I = I_0 \exp(-F_c/T), \tag{5.8}$$

where the coefficient I_0 depends on the dynamics and will be estimated in Eq. (5.22). For weal metastability, the nucleation barrier F_c/T grows as w^{-2} and I is very sensitive to w. From Eqs. (5.7) and (5.8) the nucleation barrier is expressed as

$$F_c/T = A_c/(\bar{n}/n_{\rm p} - 1)^2 \tag{5.9}$$

$$= B_c/(\chi - \chi_{\rm p})^2. \tag{5.10}$$

The two coefficients A_c and B_c are defined by

$$A_c = 16\pi\sigma^3/3\Omega^2, \tag{5.11}$$

$$B_c = 16\pi\sigma^3 v_0^2/3T^2(\phi_\alpha - \bar{\phi})^4, \tag{5.12}$$

where A_c depends on χ and $\bar{\phi}$ and B_c on $\bar{n}$ and $\bar{\phi}$. We may use Eq. (5.9) or Eq. (5.10) depending on whether $\bar{n}$ or $\chi=\chi(T)$ is varied.

In Fig. 13, we plot R_c vs $\bar{n}/n_{\rm p}-1$ at fixed χ in the left and R_c vs $\chi-\chi_{\rm p}$ at fixed $\bar{n}$ in the right. It much exceeds the molecular size a for weak metastability, where $\bar{n}/n_{\rm p}-1$ or $\chi-\chi_{\rm p}$ is small. In Fig. 14, we plot A_c at fixed χ and B_c at fixed $\bar{n}$ as functions of $\bar{\phi}$ for $g=11$. These coefficients are considerably larger than unity for $\bar{\phi}\lesssim 0.2$, but become small with increasing $\bar{\phi}$. In these figures we set $C=2T/a$. Here, notice the relations $R_c \propto C^{1/2}$, $\sigma \propto C^{1/2}$, and $F_c \propto C^{3/2}$. The coefficients A_c and B_c in Eqs. (5.11) and (5.12) depend on C as $\sigma^3 \propto \xi^3 \propto C^{3/2}$. For aqueous fluids with the hydrogen bonding network, a larger value of C might be more appropriate than in Figs. 13 and 14. See the summary for more discussions on the choice of C.

Nucleation experiments have been performed precisely on near-critical binary mixtures (without salt) [32,39–41], where appreciable droplets become observable for $F_c/T \lesssim 50$. From Fig. 14, we find $F_c/T \lesssim 50$ for $\bar{n}/n_p \gtrsim 1.2$ at $\bar{\phi}=0.1$. In our case, once $\bar{n} > n_p$ or $\chi > \chi_p$, the nucleation rate should soon become large enough for usual observations of droplets with $R > R_c$.

C. Weak metastability and droplet growth

We may derive an approximate expression for w in terms of $\bar{\phi}$ and $\bar{n}$ for weak metastablilty. To this end, we consider an equilibrium reference state, where two bulk phases with $(\phi,n)=(\phi_\alpha,n_\alpha)$ and (ϕ_β,n_β) are separated by a planar interface. We assume that the composition and the solute density (ϕ_α,n_α) in the reference phase α are the same as those within the droplet. However, those (ϕ_β,n_β) in the reference phase β are slightly different from those $(\bar{\phi},\bar{n})$ in the initial metastable state. The initial homogeneous deviations are written as

$$\delta\bar{\phi} = \bar{\phi} - \phi_\beta, \quad \delta\bar{n} = \bar{n} - n_\beta. \tag{5.13}$$

From Eqs. (2.16) and (2.17) we obtain

$$f_{\rm tot}^\alpha - f_{\rm tot}^\beta - h_{\rm cx}\Delta\phi - \mu_{\rm cx}\Delta n = 0, \tag{5.14}$$

where $f_{\rm tot}^K = f_{\rm tot}(\phi_K,n_K)$ (with $K=\alpha,\beta$). $h_{\rm cx}$ and $n_{\rm cx}$ are the values of h in Eq. (2.6) and μ in Eq. (2.7) in the reference state (which are simply written as h and μ in Sec. II). Further, we note the relation

$$\bar{f}_{\rm tot} - f_{\rm tot}^\beta - h_{\rm cx}\delta\bar{\phi} - \mu_{\rm cx}\delta\bar{n} \cong 0, \tag{5.15}$$

which is valid to first order in $\delta\bar{\phi}$ and $\delta\bar{n}$. From the first line of Eq. (5.6) we may eliminate $f_{\rm tot}^K$ and $\bar{f}_{\rm tot}$ to obtain the desired expression

$$w \cong (\bar{h} - h_{\rm cx})\Delta\phi + (\bar{\mu} - \mu_{\rm cx})\Delta n, \tag{5.16}$$

where we have set $\phi_\alpha - \bar{\phi} \cong \Delta\phi$ and $n_\alpha - \bar{n} \cong \Delta n$. From Eqs. (2.6) and (2.7) the initial deviations of the chemical potentials are expanded as

$$\bar{h} - h_{\rm cx} \cong f_\beta''\delta\bar{\phi} - Tg\delta\bar{n},$$

$$\bar{\mu} - \mu_{\rm cx} \cong T\delta\bar{n}/n_\beta - Tg\delta\bar{\phi}, \tag{5.17}$$

where f_β'' is equal to $\partial^2 f/\partial\phi^2$ at $\phi=\phi_\beta$. Therefore,

$$\frac{w}{T} \cong \left(f_\beta''\frac{\Delta\phi}{T} - g\Delta n\right)\delta\bar{\phi} + (e^{g\Delta\phi} - 1 - g\Delta\phi)\delta\bar{n}. \tag{5.18}$$

In Appendix B, we will derive the dynamic equation for the droplet radius $R(t)$ for weak metastability. It is of the standard form

$$\frac{\partial R}{\partial t} = \frac{\Lambda}{R}\left(w - \frac{2\sigma}{R}\right), \tag{5.19}$$

where Λ is a kinetic coefficient defined in Eq. (B10) below. For a dilute solute, it may be related to the mutual diffusion constant of the mixture $D_m(\phi)$ by

$$\Lambda = D_m(\bar{\phi})/f''(\bar{\phi})(\Delta\phi)^2. \tag{5.20}$$

For $R \cong R_c$ we have $\partial R/\partial t \cong \Gamma_c(R-R_c)$, where

$$\Gamma_c = 2\sigma\Lambda/R_c^3. \tag{5.21}$$

The inverse Γ_c^{-1} is the time scale of near-critical droplets. The coefficient I_0 in the nucleation rate (5.8) is determined by the droplet dynamics at $R \cong R_c$ (with appropriate thermal noises added) and is estimated as [32]

$$I_0 \sim \Gamma_c/\xi^3, \tag{5.22}$$

where ξ is the correlation length in the initial metastable state.

For $g=0$ our results tend to those for incompressible binary mixtures without salt [32,39,40]. There, we use Eq. (5.22) and the relation $w - 2\sigma/R = f_\beta''(\Delta\phi)^2[\Delta_s - 2d_0/R]$ in terms of the supersaturation $\Delta_s = \delta\bar{\phi}/\Delta\phi$ and the capillary length $d_0 = \gamma/f_\beta''(\Delta\phi)^2$.

VI. HETEROGENEOUS NUCLEATION ON HYDROPHILIC COLLOID SURFACES

In this section, we examine adsorption, wetting, and precipitation on a colloid surface. Here, the colloid surfaces are hydrophilic, while the boundary walls are hydrophobic as in the previous section. The colloid density $n_{\rm co}$ is so small that each colloid particle may be treated independently and the composition profile around it depends only on the distance r from its center. The effective cell volume for each particle is $V = n_{\rm co}^{-1}$. For simplicity, we assume that the colloids are neutral without surface charge and the correlation length ξ outside the colloids is shorter than the colloid radius d.

In Sec. III C, we have already found a prewetting transition on a planar wall for χ slightly below χ_p. Furthermore, we shall see that a wetting layer much thickens slightly above χ_p due to precipitation.

A. Simulation results: Discontinuous and continuous transitions

First, we present our numerical results for a hydrophilic particle with radius $d=15a$ or $25a$ placed at the center of a spherical cell with radius $L=10^3a$. The cell volume is $V = 4\pi L^3/3$ and the colloid volume fraction is $\phi_{\rm col} = (d/L)^3$, so $\phi_{\rm col} = 3.4\times10^{-6}$ and 1.6×10^{-5} for $d=15a$ and $25a$, respectively. We suppose hydrophilic ions using the model in Sec. IV, although the electrostatic interaction is not essential here. The other parameters used are $\bar{\phi}=0.36$, $v_0n_0 = 2\times10^{-4}$, $g_1=9$, $g_2=13$, $C=T/a$, $e^2/T=120a$, and $\varepsilon_1=\varepsilon_0=40$. The correlation length ξ far from the surface is shorter than d. In fact, it is $1.39a$ at $\chi=1.9$.

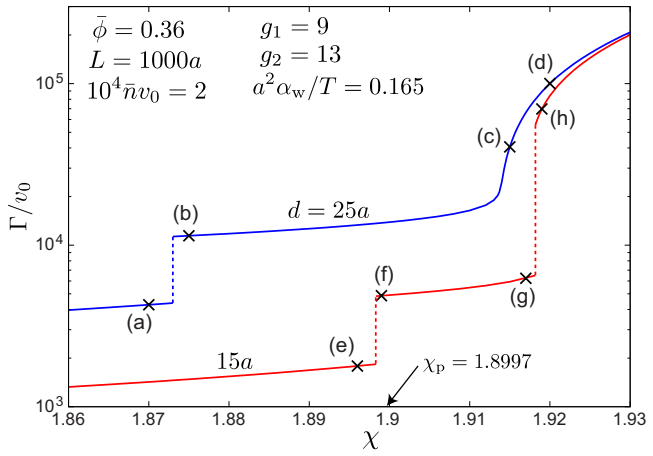

FIG. 15. (Color online) Preferential adsorption Γ on a colloid surface in Eq. (6.2) as a function of χ on a semilogarithmic scale at $\bar{\phi}=0.36$. For $d=25a$ (upper curve), after a prewetting transition at $\chi=1.873$, the crossover to precipitation is continuous. For $d=15a$ (lower curve), after a prewetting transition at $\chi=1.898$, the transition to precipitation is discontinuous at $\chi=1.918$. At points (a)–(h), the corresponding composition profiles are given in Fig. 16.

For the composition ϕ and the ion densities n_1 and n_2, the total free energy is $F_{\rm tot}=F+F_s$, where F is given by Eq. (4.4) and F_s is the surface free energy in Eq. (3.27). The composition $\phi(r)$ obeys Eq. (3.2) at a constant h. The boundary conditions at $r=d$ and L are given by

$$C\phi'(d) = -\alpha_w, \quad \phi'(L) = 0, \tag{6.1}$$

where $\phi'(r)=d\phi(r)/dr$. The wetting parameter $\alpha_{\rm w}$ is set equal to $0.165T/a^2$ as in Fig. 10.

In Fig. 15, we plot the preferential adsorption given by

$$\Gamma = \int_{r>d} d\boldsymbol{r}[\phi(r) - \phi(L)], \tag{6.2}$$

for the two diameters $d=25a$ and $15a$. It is on the order of the volume of an adsorbed layer multiplied by $\phi_\alpha - \bar{\phi}$. The prewetting transition discussed in Sec. III C occurs at $\chi=1.873$ for $d=25a$ and 1.893 for $d=15a$. Remarkably, for $\chi>\chi_{\rm p}=1.8997$, Γ increases continuously for $d=25a$, but discontinuously for $d=15a$. In Fig. 16, we show the composition $\phi(r)$ for four χ's across the transitions and around the crossover. It changes from a thin to thick wetting layer continuously (but abruptly) for $d=25a$ and discontinuously for $d=15a$. In Fig. 17, we show the free-energy change $\Delta F_{\rm tot}=F_{\rm tot}-F_{\rm tot}^0$ as a function of χ, where $F_{\rm tot}^0$ is the total free energy for the homogeneous state (realized for $\alpha_w=0$). Around the first-order transitions there appear two branches, where Eq. (3.2) is satisfied, and on the equilibrium branch $F_{\rm tot}$ takes a lower value. In particular, for $d=15a$, two branches of adsorption and precipitation appear around $\chi=1.918>\chi_{\rm p}$.

The prewetting transition point below $\chi_{\rm p}$ depends on d as in Fig. 15. Furthermore, it is slightly affected by the electric double layer for $g_1\neq n_2$. In fact, for $g_1=g_2=11$, it disappears and the prewetting transition occurs at $\chi=1.907$ for $d=25a$ and at $\chi=1.912$ for $d=15a$, while it was at $\chi=1.885$ for a planar wall in Fig. 10.

B. Theory of wetting on a colloid surface

Before the layer thickening due to precipitation and for $d\gg\xi$, $\Delta F_{\rm tot}$ is due to the adsorption expressed in terms of $\mathcal{F}_{\rm ad}$ in Eq. (3.29) as

$$\Delta F_{\rm tot} = 4\pi d^2 \mathcal{F}_{\rm ad}(\bar{\phi},\bar{n}), \tag{6.3}$$

We explicitly write the dependence of $\mathcal{F}_{\rm ad}$ on the composition $\bar{\phi}$ and the solute density $\bar{n}$ far from the surface. In Fig. 17, $\mathcal{F}_{\rm ad}$ only weakly depends on χ. After precipitation in the range $\chi>\chi_{\rm p}$, a thick wetting layer appears in the region $d<r<R$ and $\Delta F_{\rm tot}$ is expressed as

$$\Delta F_{\rm tot} = 4\pi d^2 \mathcal{F}_{\rm ad}(\phi_\alpha, n_\alpha) + F_{\rm wet}. \tag{6.4}$$

The first adsorption term is determined by the composition ϕ_α and the solute density n_α in the surrounding thick layer,

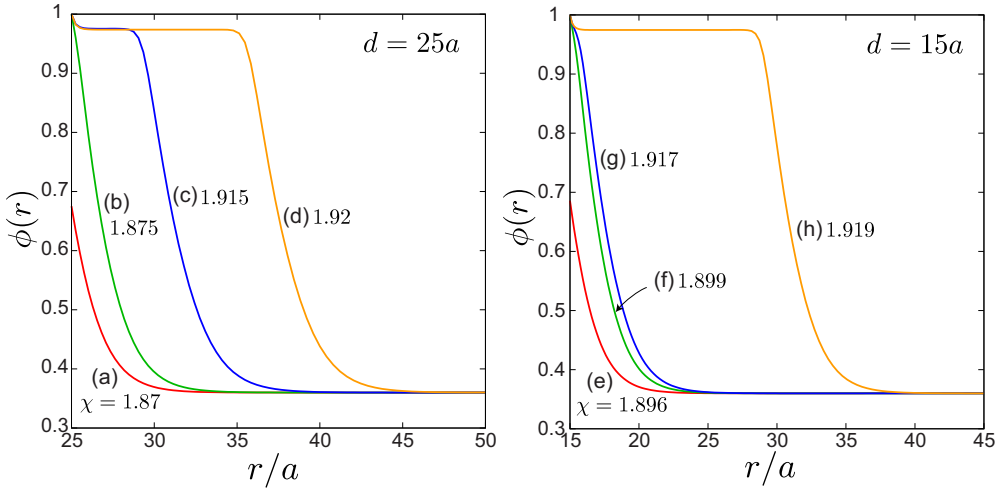

FIG. 16. (Color online) Composition $\phi(r)$ vs r/a outside a colloid $r>d$. For $d=25a$ (left), χ is (a) 1.87, (b) 1.875, (c) 1.915, and (d) 1.92. For $d=15a$ (right), χ is (e) 1.896, (f) 1.899, (g) 1.917, and (h) 1.919.

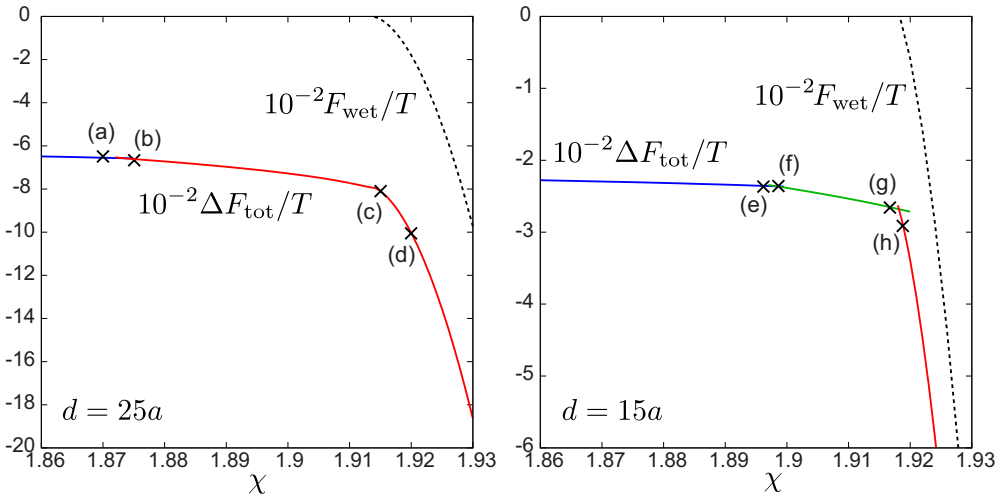

FIG. 17. (Color online) Free-energy change $\Delta F_{\rm tot}$ due to water accumulation around a colloid as a function of χ for $\bar{\phi}=0.36$. For $d=25a$ (left), after the prewetting transition between (a) and (b), the crossover to precipitation is continuous but there is an abrupt slope change at (c). For $d=15a$ (right) after the prewetting transition between (e) and (f), there is a discontinuous change between (g) and (h). Shown also is the theoretical free energy $F_{\rm wet}$ in Eq. (6.6) (dotted line).

while the second one is the contribution in the thick layer. Figure 17 indicates that $F_{\rm wet}$ decreases dramatically with increasing χ.

To construct a simple theory of $F_{\rm wet}$, we assume the condition $\Psi(\phi_\alpha)\gamma_\alpha \ll 1$ in Eq. (3.13). We treat $\Delta F_{\rm tot}$ in Eq. (3.14) as $F_{\rm wet}$. In the present situation, the volume fraction of phase α is given by

$$\gamma_\alpha = 4\pi(R^3 - d^3)/3V = (R^3 - d^3)/L^3. \tag{6.5}$$

Here, w in Eq. (3.15) is positive. In terms of the two lengths $R_c \propto w^{-1}$ in Eq. (3.18) and $R_{\rm m}$ in Eq. (3.19), we may express $F_{\rm wet}$ as

$$\frac{F_{\rm wet}}{4\pi\sigma} = R^2 - d^2 - \frac{2}{3R_c}(R^3 - d^3) + \frac{1}{3R_{\rm m}^4}(R^3 - d^3)^2$$
$$= R_{\rm m}^2\left[(q + D^3)^{2/3} - D^2 - \frac{2E}{3}q + \frac{1}{3}q^2\right]. \tag{6.6}$$

The first line follows from Eq. (3.20) if R^2 and R^3 there are replaced with $R^2 - d^2$ and $R^3 - d^3$, respectively. Thus, as $d \to 0$, this $F_{\rm wet}$ tends to $\Delta F_{\rm tot}$ in Eq. (3.20). In the second line we introduce the order parameter

$$q = (R^3 - d^3)/R_{\rm m}^3, \tag{6.7}$$

where D and E are dimensionless parameters defined as

$$D = d/R_{\rm m}, \quad E = R_{\rm m}/R_c = wR_{\rm m}/2\sigma. \tag{6.8}$$

We minimize $F_{\rm wet}$ as a function of R or q. In Fig. 17, this minimum $F_{\rm wet}$ is plotted (in dotted lines). We can see that it is larger than $\Delta F_{\rm tot}$ by a constant, as suggested by Eq. (6.4). In Fig. 18, we display q in the D-E plane, which shows how a thick wetting layer appears. For $D=0$ (or $d=0$) we have the curve of $R^3/R_{\rm m}^3$ vs $R_{\rm m}/R_c$ for a droplet with radius R (see Sec. III B for its theory).

For $R - d \gg \xi$, the adsorption free energy $4\pi d^2 \mathcal{F}_{\rm ad}$ is small as compared to $F_{\rm wet}$. Then we may examine the formation of a thick layer by minimizing $F_{\rm wet}$. For $q \ll D^3$, $F_{\rm wet}$ is expanded in powers of q as

$$\frac{F_{\rm wet}}{4\pi\sigma R_{\rm m}^2} = \frac{2}{3}\left(\frac{1}{D} - E\right)q + \left(3 - \frac{1}{D^4}\right)\frac{q^2}{9} + \frac{4q^3}{81D^7} + \cdots. \tag{6.9}$$

By setting the coefficient of q^2 equal to zero, we find a tricritical point [32], where D is given by

$$D_{\rm tri} = 3^{-1/4} = 0.760. \tag{6.10}$$

This tricritical point is at $(D,E)=(D_{\rm tri}, D_{\rm tri}^{-1})$ or at $(d,w)=(D_{\rm tri}R_{\rm m}, 2\sigma/D_{\rm tri}R_{\rm m})$. (i) For $D=d/R_{\rm m} < D_{\rm tri}$, the second term ($\propto q^2$) in expansion (6.9) is negative and the transition takes place discontinuously. The first-order transition line is

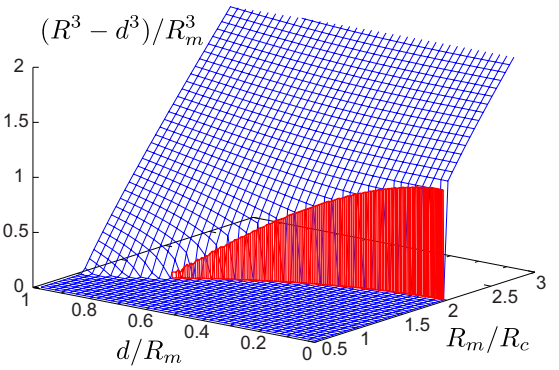

FIG. 18. (Color online) Precipitated layer volume $4\pi(R^3 - d^3)/3$ divided by $4\pi R_{\rm m}^3/3$ in the plane of $d/R_{\rm m}$ and $R_{\rm m}/R_c$. It is calculated from the approximate wetting free energy $F_{\rm wet}$ in Eq. (6.6) without the adsorption free energy $4\pi d^2 \mathcal{F}_{\rm ad}$. The transition is discontinuous for $d/R_{\rm m} < 0.760$ on the surface perpendicular to the $d/R_{\rm m}$-$R_{\rm m}/R_c$ plane (in red).

$E=E_{tr}(D)$, where $E_{tr}(D_{tri})=D_{tri}^{-1}$ and $E_{tr}(0)=2$. (ii) For $D=d/R_m>D_{tri}$, a thick wetting layer appears continuously as a second-order phase transition, where the critical line is $E=D^{-1}$. The order parameter q is nonvanishing for

$$E>D^{-1} \quad \text{or} \quad d>R_c, \tag{6.11}$$

where $q\propto(E-D^{-1})^{1/2}$ near the critical line. In Figs. 15–17, we have $R_m=26a$, so that $D=0.96>D_{tri}$ for $d=25a$ and $D=0.58<D_{tri}$ for $d=15a$. Our numerical results are consistent with the predictions from Eq. (6.6).

VII. SUMMARY AND REMARKS

In summary, we have examined solvation-induced precipitation in aqueous mixtures with a hydrophilic or hydrophobic solute in the limit of large g, which represents the composition dependence of the solvation (the strength of the preferential solvation). In Sec. II, we have developed a thermodynamic theory of two-phase coexistence in mixture solvents with a solute, numerical analysis of the two-phase coexistence, a theory of precipitation in the asymptotic limit $g\gg1$, and a theory in the dilute limit of precipitated domains. Remarkably, the precipitation curve $\chi=\chi_p$ extends far below the coexistence curve in the χ-$\bar{\phi}$ plane. In Sec. III, introducing the gradient free energy, we have calculated the surface tension σ, performed stability analysis of a precipitated droplet including the surface tension, and predicted a prewetting transition below the precipitation curve. In Sec. IV, we have presented a theory for hydrophilic ions including the solvation and electrostatic interactions. Finally, we have investigated homogeneous nucleation in Sec. V and heterogeneous nucleation on a colloid surface in Sec. VI. We have also derived the evolution equation for the droplet radius $R(t)$ from the dynamic equations for ϕ and n in metastable states in Appendix B.

We have presented a number of predictions. There are (i) droplet appearance due to preferential solvation as in Figs. 1–3, which has a minimum size R_m in Eq. (3.19), (ii) droplet size change with varying χ or T as in Fig. 11, (iii) prewetting transition slightly below the precipitation curve, (iv) nucleation slightly above the precipitation curve and far outside the solvent coexistence curve, and (v) heterogeneous nucleation on a colloid surface, where one-step or two-step first-order wetting transitions can occur as in Figs. 15–18. To confirm these effects, systematic experiments are needed, where the temperature, the water volume fraction, and the salt amount are controlled. Particularly, dynamic light scattering is informative to detect emergence of droplets and wetting on colloid surfaces. Wetted colloids should move with a smaller diffusion constant $\propto R^{-1}$.

In our theory, the molecular volumes of the two components are assumed to be given by the common v_0 in Eq. (2.4). However, they can be very different. For example, those of D_2O and 3MP (the inverse densities of the pure components) are 28 and 168 Å^3, respectively. Moreover, the coefficient C in Eq. (3.1) of the gradient free energy remains an arbitrary constant, and the nucleation rate calculated in Sec. V is proportional to $C^{3/2}$. Therefore, our theory is still very qualitative. For pure water, the observed surface tension outside the critical region $1-T/T_c\gtrsim0.1$ fairly agrees with the calculated surface tension from the van der Waals model with the gradient free-energy density $10Ta^5|\nabla n|^2/2$ [38,42], where n is the density and $a=3.1$ Å is the van der Waals radius.

In the future, we will investigate the wetting transition on charged walls, rods, and colloids and the solvation-induced colloid interaction, which can be much influenced by the ion-induced precipitation. The degree of ionization should also be treated as a fluctuating variable sensitively depending on the local environment [29].

ACKNOWLEDGMENTS

One of the authors (A.O.) would like to thank M. A. Anisimov for valuable discussions in an early stage of this work. This work was supported by Grant-in-Aid for Scientific Research on Priority Area "Soft Matter Physics" from the Ministry of Education, Culture, Sports, Science and Technology of Japan.

APPENDIX A: TWO-PHASE COEXISTENCE FOR $\chi>2$ AT VERY SMALL $\bar{n}$

For $\chi>2$ two-phase coexistence is possible without solute. Let ϕ_α^0 and ϕ_β^0 be the equilibrium volume fractions in the two phases without solute. Here, we calculate the deviations of the volume fractions $\delta\phi_\alpha=\phi_\alpha-\phi_\alpha^0$ and $\delta\phi_\beta=\phi_\beta-\phi_\beta^0$ to linear order in the solute density $\bar{n}$ in the mean-field theory. We show that the linear theory holds only for very small $\bar{n}$.

The bulk densities n_α and n_β are still given by Eqs. (2.8) and (2.9). From Eqs. (2.15) and (2.17) the chemical potential difference h is expanded as $h=-T\Delta n/\Delta\phi$, so that

$$\delta\phi_\alpha=Tn_\alpha(g\Delta\phi-1+e^{-g\Delta\phi})/f''\Delta\phi,$$

$$\delta\phi_\beta=Tn_\beta(g\Delta\phi+1-e^{g\Delta\phi})/f''\Delta\phi, \tag{A1}$$

where $f''=f''(\phi_\alpha^0)=f''(\phi_\beta^0)$ for the symmetric free-energy density in Eq. (2.4). Here, $f''(\phi)=\partial^2 f/\partial\phi^2$.

As the solvent critical point ($\chi_c=2$) is approached, the inequality $\Delta\phi\ll1/g$ holds eventually to give

$$\delta\phi_\alpha\cong-\delta\phi_\beta\cong T\bar{n}g^2\Delta\phi/2f''. \tag{A2}$$

If we set $\epsilon=\chi-2$ ($\propto1-T/T_c$), the above deviation is of order $g^2v_0\bar{n}\epsilon^{-1/2}$. The linear approximation holds when $\delta\phi_\alpha\ll\phi_\alpha^0-1/2\cong\Delta\phi/2$. Thus, the upper bound of the linear regime of the solute doping is very small as

$$\bar{n}\ll\epsilon/g^2v_0. \tag{A3}$$

In the left panels of Fig. 1, $\phi_\alpha-\phi_\beta$ is not small even for $\chi\cong2$ due to the nonlinear solute effect.

Away from the critical point, the relation $g\Delta\phi\gg1$ holds for large g. In this case, we find

$$\delta\phi_\alpha\cong Tgn_\alpha/f'', \quad \delta\phi_\beta\cong-Tn_\alpha/f''\Delta\phi, \tag{A4}$$

so that $\delta\phi_\alpha\cong-(g\Delta\phi)\delta\phi_\beta>0$. From Eq. (2.13) $\delta\phi_\alpha(\propto n_\alpha)$ increases steeply as $\bar{\phi}$ is decreased to ϕ_β^0 (or as γ_α is decreased). This tendency can be seen in the left panels of Fig.

1. The maximum of n_α is $\bar{n}e^{g\Delta\phi}$. The condition that $\delta\phi_\alpha$ is much smaller than unity is written as

$$\bar{n} \ll f'' e^{-g\Delta\phi}/Tg. \tag{A5}$$

If Eq. (A3) or Eq. (A5) does not hold, ϕ_α nonlinearly deviates from ϕ_α^0 with respect to $\bar{n}$.

APPENDIX B: DROPLET GROWTH

For weak metastability, we derive the droplet-evolution equation (5.19) in the neutral solute case. The simplest dynamic equations for the composition $\phi(\boldsymbol{r},t)$ and the solute density $n(\boldsymbol{r},t)$ are given by the diffusive equations

$$\frac{\partial \phi}{\partial t} = L\nabla^2(h - C\nabla^2\phi), \tag{B1}$$

$$\frac{\partial n}{\partial t} = D_s \nabla \cdot n \nabla \cdot (\mu/T), \tag{B2}$$

where L is the kinetic coefficient for the composition, D_s is the solute diffusion constant, and h and μ are given in Eqs. (2.6) and (2.7). Around a spherical droplet with radius R, all the quantities depend on the distance r from the droplet center and the time t.

Slightly outside the droplet surface $r-R \gtrsim \xi$, the gradient term in h is negligible, where ξ is the interface thickness. When the droplet growth or shrinkage is slow, we may use the quasistatic approximation:

$$h \cong \bar{h} + (h_R - \bar{h})R/r,$$

$$\mu \cong \bar{\mu} + (\mu_R - \bar{\mu})R/r, \tag{B3}$$

where h and μ tend to $\bar{h}$ and $\bar{\mu}$ far from the droplet and to h_R and μ_R near the droplet surface. The conservations of ϕ and n at the interface yield

$$\frac{\partial R}{\partial t}\Delta\phi = \frac{L}{R}(h_R - \bar{h}),$$

$$\frac{\partial R}{\partial t}\Delta n = \bar{n}\frac{D_s}{R}(\mu_R - \bar{\mu}), \tag{B4}$$

where $\Delta\phi = \phi_\alpha - \phi_\beta$ and $\Delta n = n_\alpha - n_\beta$ as in Eq. (2.13).

In the interface region $|r-R| \lesssim \xi$, the generalized chemical potential $\mu - C\nabla^2\phi$ including the gradient term may be treated as a constant h_R, so that

$$h_R = h - C\left(\frac{\partial^2}{\partial r^2} + \frac{2}{r}\frac{\partial}{\partial r}\right)\phi. \tag{B5}$$

The solute chemical potential μ is also a constant μ_R near the interface. We set $\phi = \phi_{\rm int}(r-R) + \delta\phi$ and $n = n_{\rm int}(r-R) + \delta n$ in the interface region. Here, $\phi_{\rm int}(z)$ is the one-dimensional interface solution of Eq. (3.4) and $n_{\rm int}(z) = n_\beta e^{g[\phi_{\rm int}(z)-\phi_\beta]}$. These represent the reference profiles and the corresponding h and μ are written as $h_{\rm cx}$ and $\mu_{\rm cx}$ as in Eq. (5.14). To linear order in $\delta\phi$ and δn, we obtain $\mu_R - \mu_{\rm cx} = T\delta n/n_{\rm int} - Tg\,\delta\phi$ or

$$\delta n = n_{\rm int}[(\mu_R - \mu_{\rm cx})/T + g\,\delta\phi], \tag{B6}$$

in the region $|r-R| \lesssim \xi$. We may linearize Eq. (B5) as

$$h_R - h_{\rm cx} = \left[f''(\phi_{\rm int}) - Tg^2 n_{\rm int} - C\frac{\partial^2}{\partial r^2}\right] \times \delta\phi - \frac{2}{R}C\phi'_{\rm int} - g(\mu_R - \mu_{\rm cx})n_{\rm int}. \tag{B7}$$

Then we multiply Eq. (B7) by $\phi'_{\rm int} = d\phi_{\rm int}(r-R)/dr$ and integrate over the region $|r-R| \lesssim \xi$ to obtain

$$(h_R - h_{\rm cx})\Delta\phi \cong \frac{2\sigma}{R} - (\mu_R - \mu_{\rm cx})\Delta n, \tag{B8}$$

where the first term in the right-hand side of Eq. (B7) does not contribute and use has been made of Eq. (3.9) and $gn_{\rm int}\phi'_{\rm int} = dn_{\rm int}/dr$. We rewrite Eq. (B8) as

$$(h_R - \bar{h})\Delta\phi + (\mu_R - \bar{\mu})\Delta n \cong \frac{2\sigma}{R} - w, \tag{B9}$$

where w is given in Eq. (5.16) in the linear form. Using Eq. (B4) we eliminate $h_R - \bar{h}$ and $\mu_R - \bar{\mu}$ from Eq. (B9) to obtain the droplet evolution equation (5.19) with

$$1/\Lambda = (\Delta\phi)^2/L + (\Delta n)^2/D_s\bar{n}, \tag{B10}$$

where the second term in the right-hand side is negligible for dilute solute, leading to $\Lambda \cong L/(\Delta\phi)^2$ and Eq. (5.20).

[1] E. L. Eckfeldt and W. W. Lucasse, J. Phys. Chem. **47**, 164 (1943); B. J. Hales, G. L. Bertrand, and L. G. Hepler, *ibid.* **70**, 3970 (1966).

[2] V. Balevicius and H. Fuess, Phys. Chem. Chem. Phys. **1**, 1507 (1999).

[3] T. Narayanan and A. Kumar, Phys. Rep. **249**, 135 (1994).

[4] J. Jacob, A. Kumar, S. Asokan, D. Sen, R. Chitra, and S. Mazumder, Chem. Phys. Lett. **304**, 180 (1999).

[5] M. Misawa, K. Yoshida, K. Maruyama, H. Munemura, and Y. Hosokawa, J. Phys. Chem. Solids **60**, 1301 (1999).

[6] J. Jacob, A. Kumar, M. A. Anisimov, A. A. Povodyrev, and J. V. Sengers, Phys. Rev. E **58**, 2188 (1998); M. A. Anisimov, J. Jacob, A. Kumar, V. A. Agayan, and J. V. Sengers, Phys. Rev. Lett. **85**, 2336 (2000).

[7] T. Takamuku, A. Yamaguchi, D. Matsuo, M. Tabata, M. Kumamoto, J. Nishimoto, K. Yoshida, T. Yamaguchi, M. Nagao, T. Otomo, and T. Adachi, J. Phys. Chem. B **105**, 6236 (2001).

[8] K. Jurkiewicz, Fluid Phase Equilib. **251**, 24 (2007).

[9] G. W. Euliss and C. M. Sorensen, J. Chem. Phys. **80**, 4767 (1984); Y. Georgalis, A. M. Kierzek, and W. Saenger, J. Phys. Chem. B **104**, 3405 (2000); A. F. Kostko, M. A. Anisimov, and J. V. Sengers, Phys. Rev. E **70**, 026118 (2004); M. Wag-

ner, O. Stanga, and W. Schröer, Phys. Chem. Chem. Phys. **6**, 580 (2004); C. Yang, W. Li, and C. Wu, J. Phys. Chem. B **108**, 11866 (2004); M. Sedlak, *ibid.* **110**, 4329 (2006); **110**, 4339 (2006); **110**, 13976 (2006); F. Jin, J. Ye, L. Hong, H. Lam, and C. Wu, *ibid.* **111**, 2255 (2007).

[10] J. Jacob, M. A. Anisimov, J. V. Sengers, A. Oleinikova, H. Weingärtner, and A. Kumar, Phys. Chem. Chem. Phys. **3**, 829 (2001).

[11] The dynamic scattering intensity $G(q,t)$ consists of the contribution from the composition fluctuations and that from the heterogeneities. The latter is proportional to $\phi_h R^3 \exp(-D_R q^2 t)$ for wave number q. Here, the heterogeneities have a radius $R \ll 2\pi/q$ at a volume fraction $\phi_h \ll 1$. The diffusion constant D_R is given by the Stokes formula ($\propto R^{-1}$).

[12] D. Bonn, D. Ross, S. Hachem, S. Gridel, and J. Meunier, EPL **58**, 74 (2002).

[13] K. Sadakane, H. Seto, H. Endo, and M. Shibayama, J. Phys. Soc. Jpn. **76**, 113602 (2007); K. Sadakane, A. Onuki, K. Nishida, S. Koizumi, and H. Seto, Phys. Rev. Lett. **103**, 167803 (2009).

[14] P. G. Arscott, C. Ma, J. R. Wenner, and V. A. Bloomfield, Biopolymers **36**, 345 (1995); A. Hultgren and D. C. Rau, Biochemistry **43**, 8272 (2004); C. Stanley and D. C. Rauy, Biophys. J. **91**, 912 (2006).

[15] M. E. Leunissen, A. van Blaaderen, A. D. Hollingsworth, M. T. Sullivan, and P. M. Chaikin, Proc. Natl. Acad. Sci. U.S.A. **104**, 2585 (2007); M. E. Leunissen, J. Zwanikken, R. van Roij, P. M. Chaikin, and A. van Blaaderen, Phys. Chem. Chem. Phys. **9**, 6405 (2007).

[16] J. de Graaf, J. Zwanikken, M. Bier, A. Baarsma, Y. Oloumi, M. Spelt, and R. van Roij, J. Chem. Phys. **129**, 194701 (2008).

[17] J. N. Israelachvili, *Intermolecular and Surface Forces* (Academic Press, London, 1991).

[18] T. Osakai and K. Ebina, J. Phys. Chem. B **102**, 5691 (1998).

[19] D. N. Shin, J. W. Wijnen, J. B. F. N. Engberts, and A. Wakisaka, J. Phys. Chem. B **106**, 6014 (2002); H. Kobara, A. Wakisaka, K. Takeuchi, and T. Ibusuki, *ibid.* **107**, 11827 (2003).

[20] J. L. Tveekrem and D. T. Jacobs, Phys. Rev. A **27**, 2773 (1983).

[21] D. Beaglehole, J. Phys. Chem. **87**, 4749 (1983); see Ref. [34] for discussions on this work.

[22] A. Onuki and H. Kitamura, J. Chem. Phys. **121**, 3143 (2004).

[23] A. Onuki, Phys. Rev. E **73**, 021506 (2006); J. Chem. Phys. **128**, 224704 (2008).

[24] G. Marcus, S. Samin, and Y. Tsori, J. Chem. Phys. **129**, 061101 (2008).

[25] M. Bier, J. Zwanikken, and R. van Roij, Phys. Rev. Lett. **101**, 046104 (2008); J. Zwanikken, J. de Graaf, M. Bier, and R. van Roij, J. Phys.: Condens. Matter **20**, 494238 (2008).

[26] D. Ben-Yaakov, D. Andelman, D. Harries, and R. Podgornik, J. Phys. Chem. B **113**, 6001 (2009).

[27] T. Araki and A. Onuki, J. Phys.: Condens. Matter **21**, 424116 (2009); A. Onuki, T. Araki, and R. Okamoto, J. Phys.: Condens. Matter (to be published).

[28] B. Rotenberg, I. Pagonabarragac, and D. Frenkel, Faraday Discuss. **144**, 223 (2010).

[29] A. Onuki and R. Okamoto, J. Phys. Chem. B **113**, 3988 (2009); R. Okamoto and A. Onuki, J. Chem. Phys. **131**, 094905 (2009).

[30] A. Onuki, EPL **82**, 58002 (2008).

[31] A. Onuki, in *Polymer, Liquids and Colloids in Electric Fields: Interfacial Instabilities, Orientation and Phase-Transitions*, edited by Y. Tsori (World Scientific, Singapore, 2009).

[32] A. Onuki, *Phase Transition Dynamics* (Cambridge University Press, Cambridge, England, 2002).

[33] J. W. Cahn, J. Chem. Phys. **66**, 3667 (1977).

[34] P. G. de Gennes, Rev. Mod. Phys. **57**, 827 (1985).

[35] L. Onsager and N. N. T. Samaras, J. Chem. Phys. **2**, 528 (1934); Y. Levin and J. E. Flores-Mena, EPL **56**, 187 (2001).

[36] L. Q. Hung, J. Electroanal. Chem. **115**, 159 (1980).

[37] If the water volume fraction ϕ is increased from zero in oil, a solvation shell is gradually created around each hydrophilic ion for $\phi < \phi_{sol}$, where ϕ_{sol} is a very small crossover volume fraction. Expression (4.5) holds only for $\phi > \phi_{sol}$ and is not applicable for $\phi < \phi_{sol}$.

[38] H. Kitamura and A. Onuki, J. Chem. Phys. **123**, 124513 (2005).

[39] J. S. Langer and A. J. Schwartz, Phys. Rev. A **21**, 948 (1980).

[40] A. J. Schwartz, S. Krishnamurthy, and W. I. Goldburg, Phys. Rev. A **21**, 1331 (1980); R. G. Howland, N.-C. Wong, and C. M. Knobler, J. Chem. Phys. **73**, 522 (1980).

[41] E. D. Siebert and C. M. Knobler, Phys. Rev. Lett. **52**, 1133 (1984).

[42] S. B. Kiselev and J. F. Ely, J. Chem. Phys. **119**, 8645 (2003).